Andean Geology 52 (2): 239-253. May, 2025
doi: 10.5027/andgeoV52n2-3723

Andean Geology
www.andeangeology.cl

Assessing permafrost structures in headwater aquifers: an example from the Ojos del Salado massif, Andes mountains

***Sebastián Ruiz Pereira[1, 2], Sarah Leray[1, 3], Etienne Marti[1], Eneko Beriain[4, 5], Francisco Suárez[1], Gonzalo Yáñez[6], Balázs Nagy[7]**

[1] *Departamento de Ingeniería Hidráulica y Ambiental, Pontificia Universidad Católica de Chile, av. Vicuña Mackenna 4860, Macul, Santiago, Chile. ORCID: 0000-0002-5118-5143.*
spruiz@uc.cl, saleray@uc.cl, ebmarti@uc.cl, fsuarez@uc.cl

[2] *PermaChile network, Földgömb Foundation, balazs@afoldgomb.hu, Kunigunda útja 18, Budapest, Hungary.*

[3] *Centro de Cambio Global, Pontificia Universidad Católica de Chile, av. Vicuña Mackenna 4860, Macul, Santiago, Chile.*

[4] *GeoNomadic, Biarritz 1919, Providencia, Santiago, Chile.*

[5] *Geoestudios, Los Aromos 3371, Las Vertientes, San José de Maipo, Chile.*
eberiain@geoestudios.cl

[6] *Pontificia Universidad Católica de Chile, av. Vicuña Mackenna 4860, Macul, Santiago, Chile.*
gyaneza@uc.cl

[7] *Department of Physical Geography, Eötvös Loránd University, Pázmány Péter stny. 1, Budapest, Hungary.*
balazs.nagy@ttk.elte.hu

* *Corresponding author: spruiz@uc.cl*

ABSTRACT. In arid regions, the hydrological evolution of high mountains is a matter of concern under current climate forcing and increasing freshwater demand. Mountain surface hydrology is key for water storage and release and determines the amount and quality of freshwater supply for downstream ecosystems, so predicting their evolution under climate change scenarios requires detailed spatial data on subsurface hydrodynamic properties.In the present contribution, a semi-direct characterization of periglacial areas and permafrost zonation was carried out along an altitudinal transect at the Ojos del Salado massif (27°06' S; 68°32' W) between 4,550 and 5,830 m a.s.l. by integrating geophysics (electrical resistivity tomography; ERT) and decade-long surface temperature datasets. ERT data evidence a permafrost altitudinal gradient from a negative control at 4,550 m a.s.l. up to consistent (>100 kΩm) permafrost-related resistivities above 5,260 m a.s.l. These resistivity structures are assumed to act as confining layers, accounting for thicknesses of 8 and 25 m at the Atacama (5,260 m a.s.l.) and Tejos (5,830 m a.s.l.) sites, respectively. The geophysically determined permafrost distribution is coherent with temperature-based Frost number estimates at all sites surveyed.The results presented here are required for aquifer parameterization under short- and mid-term hydrological connectivity changes, being therefore relevant for a better understanding of groundwater storage dynamics upon permafrost degradation in arid regions.

Keywords: Mountain permafrost, High Andes, Ojos del Salado massif, Periglacial aquifer, Electrical Resistivity Tomography.

RESUMEN. Evaluación de estructuras de permafrost en acuíferos de cabecera: un ejemplo del macizo Ojos del Salado, Cordillera de los Andes. En regiones áridas, la evolución hidrológica en alta montaña es un tema de preocupación bajo el actual forzamiento climático y la creciente demanda de agua dulce. En las montañas, la hidrología superficial es clave para el almacenamiento y liberación de agua, lo cual determina la cantidad y la calidad del suministro de agua dulce para ecosistemas aguas abajo, por lo que predecir su evolución bajo escenarios de cambio climático requiere información detallada sobre las propiedades hidrodinámicas del subsuelo. En la presente contribución se efectúa una caracterización semidirecta de las áreas periglaciares y de la zonificación del permafrost a lo largo de un transecto altitudinal en el macizo Ojos del Salado (27°06' S; 68°32' O) entre los 4.550 y 5.830 m s.n.m., mediante la integración de datos geofísicos (tomografía de resistividad eléctrica; ERT en inglés) y de temperatura superficial a escala decadal. Los datos de ERT evidencian para el permafrost un gradiente altitudinal a partir de un control negativo a 4.550 m s.n.m. hasta resistividades del orden de >100 kΩm por encima de los 5.260 m s.n.m. Estas estructuras altamente resistivas actuarían como capas de confinamiento, con espesores estimados de 8 y 25 m en los sectores de Atacama (5.260 m s.n.m.) y Tejos (5.830 m s.n.m.), respectivamente. La distribución del permafrost según estos datos geofísicos es coherente con las estimaciones del Número de Escarcha (Frost number en inglés) para todos los sitios estudiados. Los resultados presentados aquí son necesarios para la parametrización de los acuíferos bajo cambios de conectividad hidrológica en el corto y mediano plazo, por lo tanto, son relevantes para mejorar el entendimiento de la dinámica del almacenamiento de agua subterránea ante escenarios de degradación de permafrost en regiones áridas.

Palabras clave: Permafrost de montaña, Cordillera de los Andes, Macizo Ojos del Salado, Acuífero periglaciar, Tomografía de resistividad eléctrica.

1. Introduction

Understanding groundwater systems in remote high mountain contexts often involves exploring and identifying aquifers within complex geological deposits (Meju, 2002), frequently with scarce to nonexistent previous information (Bishop *et al.*, 2008). The spatial distribution and characterization of aquifer confining layers at high-altitude sites is crucial for assessing the impact of freeze-thaw cycle dynamics or long-term permafrost degradation on headwaters and consequently, on downstream ecosystems (Bense *et al.*, 2009). For instance, changes in vertical leakage within these aquifers can lead to alterations in the mixing regimes (Ravenscroft *et al.*, 2005) and hydraulic feedback for assessing groundwater response times, resilience, and quality of freshwater supply (Cuthbert *et al.*, 2019; Perrone and Jasechko, 2019; Gleeson *et al.*, 2020; Jasechko and Perrone, 2021), which are particularly critical under climate change scenarios in arid regions (Leray *et al.*, 2013).

Assessing such issues in remote, scarcely monitored permafrost natural systems, facilitates visualizing future hydrological pathways in regions undergoing cryosphere degradation (Jorgenson *et al.*, 2001; Jin *et al.*, 2021). For example, high-altitude settings (>5,000 m a.s.l.) in the dry Andes (Fig. 1) enable colder, drier conditions, which under the Sixth Assessment Report (AR6) of the United Nations Intergovernmental Panel on Climate Change (IPCC) 50-year future warming scenario (IPCC, 2023), could change subsurface ice content and ground freezing duration due to snowmelt rate and partitioning (Musselman *et al.*, 2017; Hammond *et al.*, 2019). Consequently, groundwater flow path rerouting, affecting both subsurface confinement (Cochand *et al.*, 2020) and annual groundwater discharge (Somers and McKenzie, 2020), is expected.

In frost-prone areas, such as periglacial environments, the disruption of natural flow systems upon surface warming (*e.g.*, permafrost thaw) may impact the organization of groundwater flow components (Zinn and Konikow, 2007), as freezing temperatures modify water infiltration into the frozen subsurface (Liao and Zhuang, 2017; Uhlemann *et al.*, 2021). Therefore, an adequate appraisal of such processes requires assessing recharge variability and active layer thicknesses, as seasonal fluctuations of unconfined groundwater levels affect aquifer volume (Bethke and Johnson, 2008) and groundwater residence times (Bethke and Johnson, 2002).

In Andean permafrost areas (Bartsch *et al.*, 2016; Obu *et al.*, 2019), such as the Ojos del Salado massif (OSM) in northern Chile (27°06' S, 68°32' W; Fig. 1), future thaw of interstitial ice could impact aquifer recharge, as near surface, low-permeability permafrost conditions strongly affect the distribution

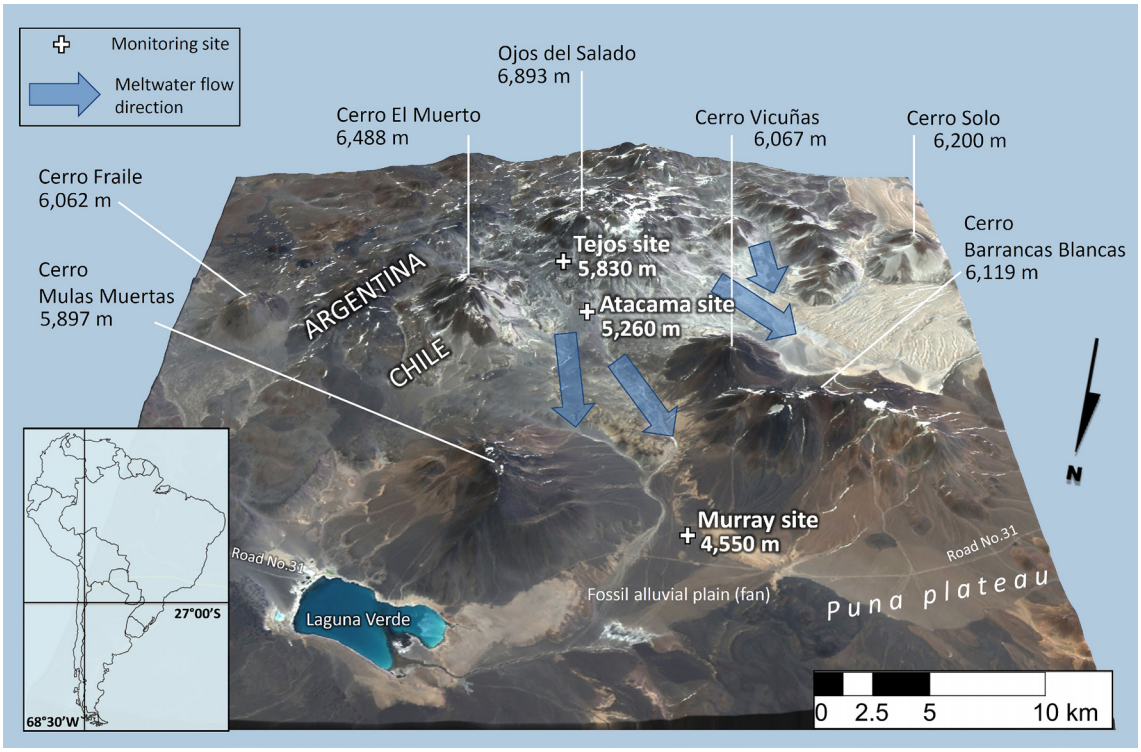

FIG. 1. Study area in the dry Andes of northern Chile. Geophysically surveyed sites (white crosses) are shown north from the Ojos del Salado massif. The map scale decreases by about 15% from front to back. North arrow points downwards.

of hydraulic heads and associated fluid flow patterns (*e.g.*, Bense and Person, 2008). Therefore, the role of permafrost in mountain hydrology should ideally be more relevant to water budget (Arenson *et al.*, 2022), as permafrost thaw results in the deepening of aquitard roofs, allowing deeper flow paths and causing a decrease in summer stream temperatures and evapotranspiration in headwater catchments (Sjöberg *et al.*, 2021).

The present work aims to unveil permafrost structures in high-altitude aquifers along an altitudinal gradient (4,550-5,830 m a.s.l.) at the OSM, a cryosphere-relevant massif in the dry Andes of South America, which may present different cryo-hydrogeological configurations (Fig. 2) and other hillslope permafrost environments (Evans and Ge, 2017). Different locations were assessed along a NNW-SSE transect, from an inferred no-permafrost condition at the warmest, lowest altitude site (4,550 m a.s.l.), an inferred sporadic permafrost condition at an intermediate altitude site (5,260 m a.s.l.), and a positive control for permafrost at the coldest, highest site (5,830 m a.s.l.) (Fig. 2). A standard methodology was used to characterize permafrost areas by contrasting electrical resistivities outlining the active layer depth (seasonal ground thaw) and permafrost table (perennially frozen ground) to interpret the current relevant subsurface architecture.

2. Study area and methods

The study area was chosen since there are neither permafrost altitudinal zonation assessments nor subsurface characterization of permafrost thicknesses. At each site, electrical resistivity tomography (ERT) data (Krautblatter and Hauck, 2007; Hilbich *et al.*, 2021; Buckel *et al.*, 2022) were integrated along with permafrost probability estimates (Ran *et al.*, 2015) derived from long-term ground temperature datasets (Fig. 3). Such a geophysical survey covering different altitudes at sites with decade-long surface temperature data is unprecedented in the Andes.

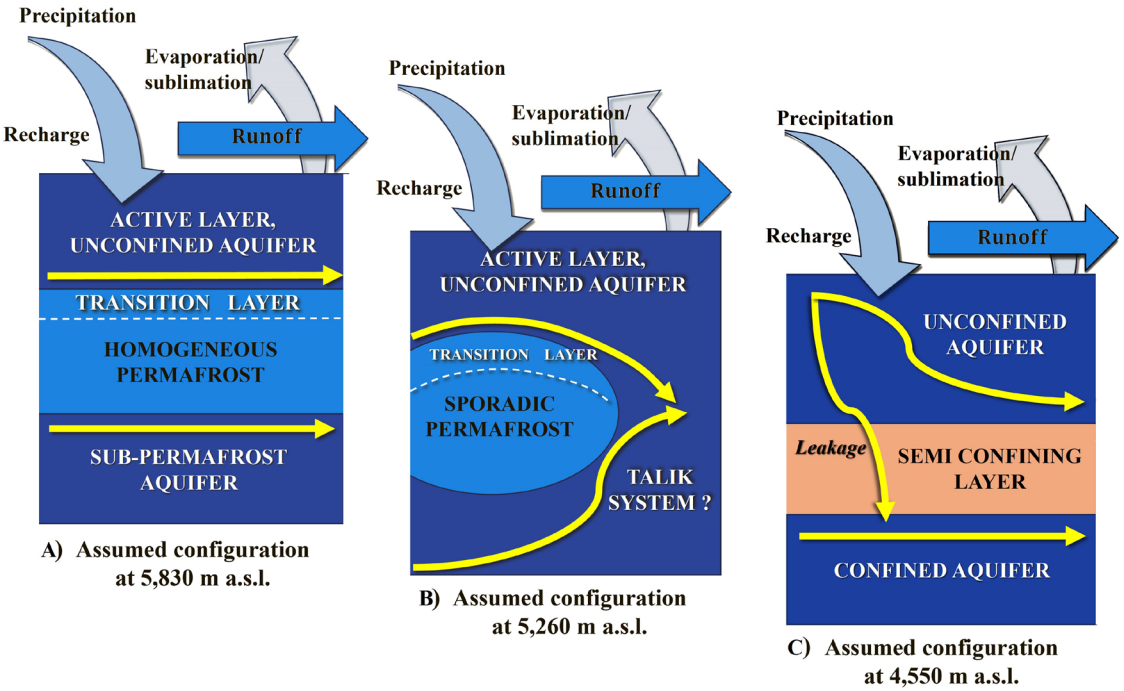

FIG. 2. Conceptual subsurface structures at the Ojos del Salado transect (see Fig. 1 for location of sites). Arrows represent idealized flow paths. **A.** Highest-altitude, colder configuration with consistent, homogeneous permafrost distribution. **B.** Configuration with isolated permafrost distribution and possibly the lower permafrost limit. **C.** Warmer areas, water leakage and negative permafrost control configuration.

2.1. Characteristics of the study area

The study area is located around the Ojos del Salado volcano (6,893 m a.s.l.), which is the highest massif of the dry Andes. The Ojos del Salado massif (OSM) and its immediate surroundings are part of the mountain desert and tundra belt of the high Andes of northern Chile. Therefore, the massif lacks active glaciers, showing only perennial snow/firn patches. The thermal climatic snowline runs at an altitude of about 7,000 m a.s.l. (Houston and Hart, 2004), and precipitation is dominated by thin winter snow cover only for a few weeks between May and October (Kereszturi *et al.*, 2022). The massif has a predicted permafrost condition (>0.5 probability) above 5,000 m a.s.l. (Bartsch *et al.*, 2016). Additionally, thermokarst features near the Atacama site at 5,260 m a.s.l. are present, including buried ice layers (Kereszturi *et al.*, 2022).

Regolith thicknesses around the established transects account for several meters of coarse-grained volcanic debris. Wind erosion, transport, and deposition are the most active surface processes at the study sites (Nagy *et al.*, 2019), where the boulders show marked features of wind abrasion. Evidence of periglacial cryoturbation and frost heave is absent on these surfaces, while slope processes are present only above ~5,600 m a.s.l. (Nagy *et al.*, 2019).

According to temperature monitoring data between 2012 and 2023, the study sites show an overall warming soil temperature trend (Fig. 4). In fact, the mean warming was about 0.03 °C/month at the Murray site, 0.012 °C/month at the Atacama site, and 0.006 °C/month at the Tejos site. Satellite-based snow cover studies show no winter cover at Murray and a predominant winter cover at both Atacama and Tejos, with the latter presenting an occasional snow cover in mid-summer (Nagy *et al.*, 2019, 2023).

The composition and characteristics of the substrate for each study site are explained below. We provide bulk density and porosity estimates for the three sites and relative and absolute humidity values for Murray.

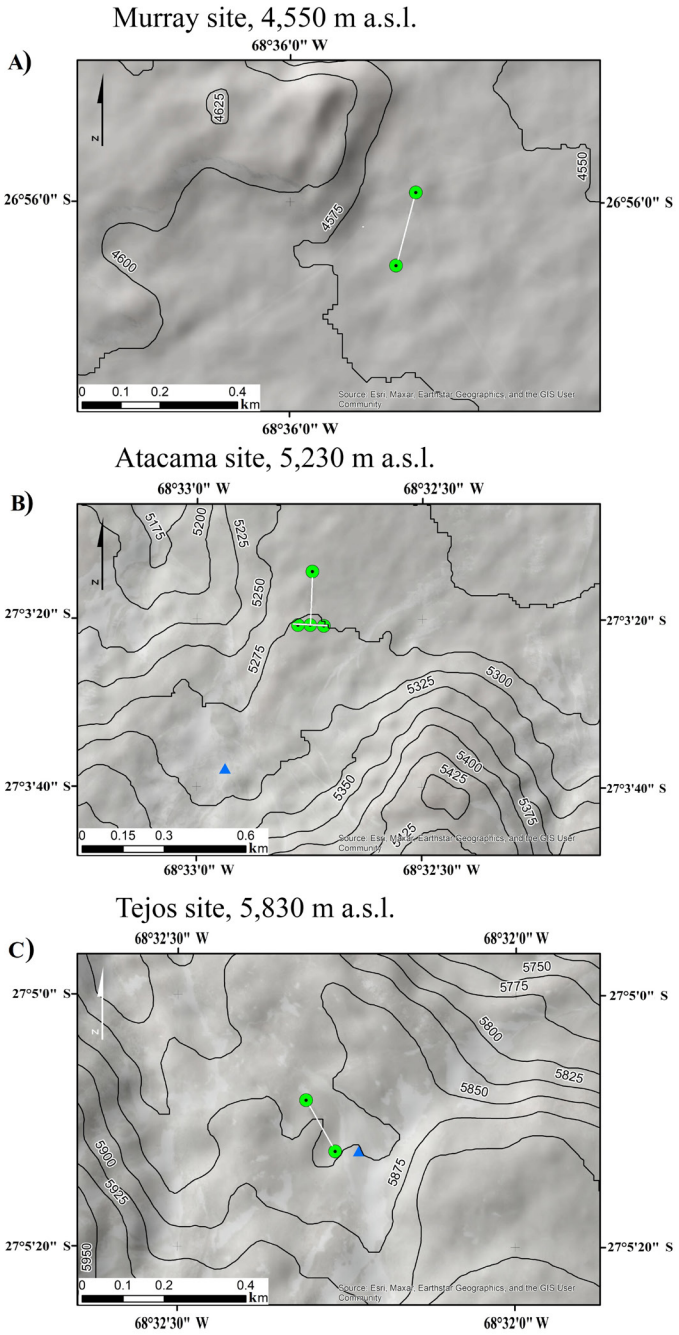

FIG. 3. Geophysically surveyed areas at the Ojos del Salado massif (**A**: Murray; **B**: Atacama; **C**: Tejos). Electrical resistivity tomography transects (green circles, white lines) and water sample locations (blue triangles) are shown for each site. The Atacama site has two perpendicular transects: a longer (195 m) N-S and a shorter (95 m) E-W. Contour lines every 25 m.

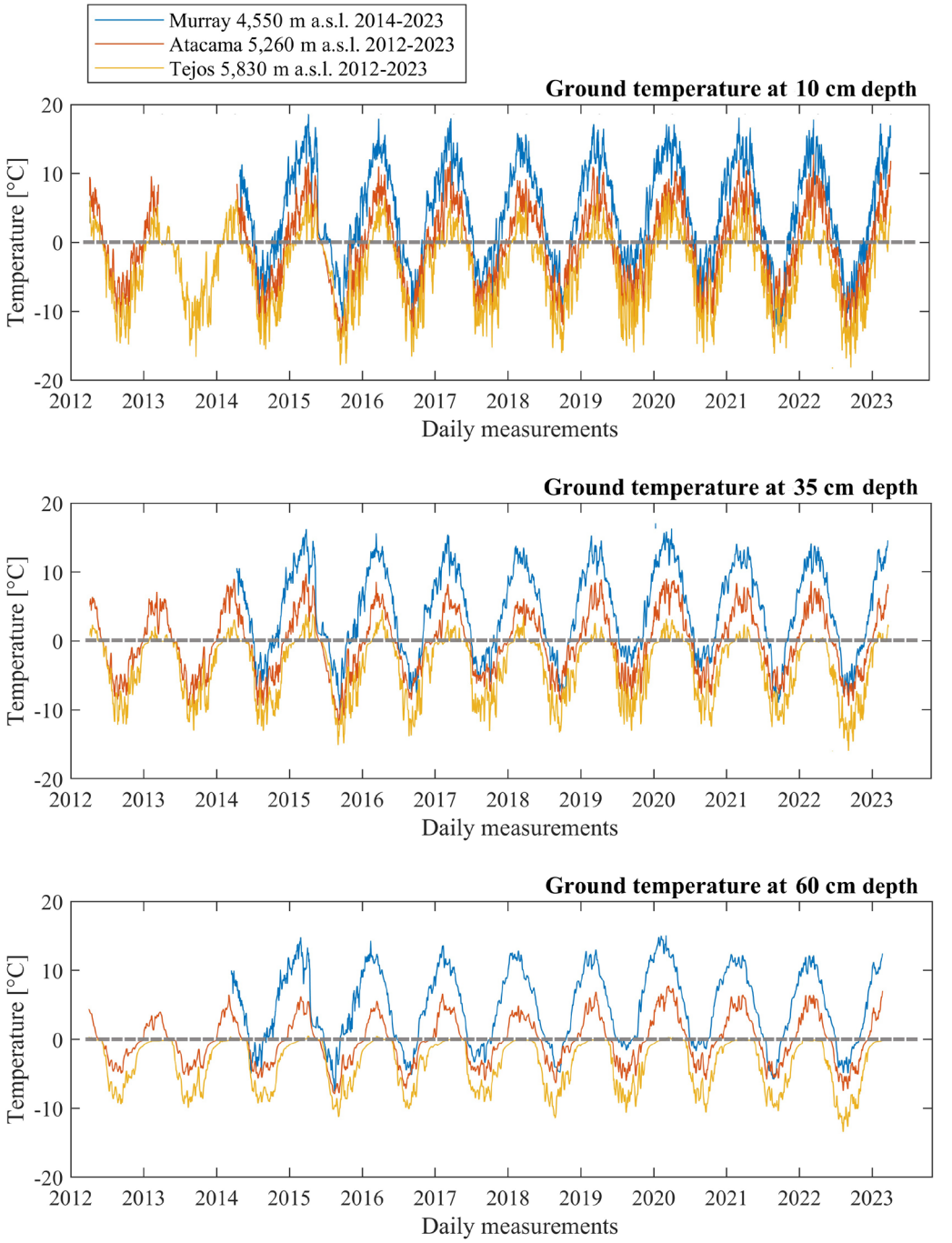

FIG. 4. Daily temperature time series at Murray (blue line), Atacama (red line), and Tejos (yellow line) for three different depths, during a 9- to 11-year period. Ground surface temperature datasets extracted from the PermaChile network (www.permachile.com).

2.1.1. Murray site

The Murray site is located ~20 km northwards from the OSM at 4,550 m a.s.l., in a pediment surface developed on the central part of a fossil alluvial fan. There are neither watercourses nor evident drainage lines around the site. The largest clasts on the surface are cm-sized pumice fragments. The bulk density and porosity of the regolith were determined following Nagy *et al.* (2019), and resulted in 1.4 g/cm^3 at 10 cm, 1.5 g/cm^3 at 35 cm, and 1.4 g/cm^3 at 60 cm depth, and 21-25% v/v for the same depth range (the lowest porosities of all sites surveyed). The relative humidity was measured by means of a HOBO Pro v2 Temperature/Relative Humidity logger on an hourly basis. At 10 cm depth, it drops to 47% in summer with an absolute humidity value of 3.75 g/m^3.

2.1.2. Atacama site

The Atacama site is located ~5.5 km northwards from the OSM at 5,260 m a.s.l., in a flat lava plain. It is only above this site that slopes become relevant (see Fig. 1). The site is characterized by extensive megaripple fields, which extend across the rocky outcrop interspersed with large, wind-carved boulders (Nagy *et al.*, 2019, 2020). The surveyed area is rich in pumice fragments with a well-developed lag gravel pavement, and at about 35 cm depth the regolith's >2 mm diameter fraction is dominant. In the 60 cm depth range, the porosity of the sediment is 50-55% v/v and the water absorption capacity (calculated following Nagy *et al.*, 2019) is high only in the upper 10 cm (1,081 nm) and then drastically decreases with depth. The bulk density of the regolith is 1.3 g/cm^3 at a depth of 10 cm and 1.5 g/cm^3 at depths of 35 and 60 cm. Below 40 cm depth, rock fragments larger than 10 cm appear and the sediment becomes highly compact. Evidence of cryoturbation was not observed (Nagy *et al.*, 2019).

At this site, the phase-change model of Nagy *et al.* (2020) applied to the near-surface (first 100 cm depth) regolith showed that the active layer is at least >1 m-thick. No evident ice was detected, but the model suggested that permafrost was a possibility. Mean annual temperatures are typically close to 0 °C, although warmer temperatures were sometimes recorded at all depths (Table 1). The number of days with temperatures above 0 °C decreases with depth and increases at lower altitudes (Table 1). These temperature data indicate that the presumed subsurface permafrost at Atacama may play a role in keeping the regolith frozen during specific periods. At a depth of 60 cm, the proportion of freeze-thaw cycle days (*i.e.*, days when the air temperature fluctuates between freezing and non-freezing temperatures) estimated at Atacama decreases to a third of that estimated at Murray (Table 1).

According to Nagy *et al.* (2019, 2020), thawing starts in mid-October and the surface freezes again in early to mid-April. It takes 40-50 days to thaw the first 100 cm and refreezing is delayed by about

TABLE 1. THERMAL DATA FOR THE THREE STUDY SITES IN THE OJOS DEL SALADO MASSIF.

	Site	10 cm depth	35 cm depth	60 cm depth
Mean annual ground temperature (°C)	Murray	4.47	4.49	4.81
	Atacama	0.35	0.16	-0.08
	Tejos	-3.58	-3.52	-3.3
Thawing degree-days	Murray	251	251	269
	Atacama	164	153	142
	Tejos	103	72	14
Percentage of freeze-thaw cycles	Murray	27	4.8	1.8
	Atacama	23	1.5	0.6
	Tejos	16.3	2.2	0.6

The temperature record period was 2014-2023 for the Murray site (4,550 m a.s.l.) and 2012-2023 for the Atacama (5,260 m a.s.l.) and Tejos (5,830 m a.s.l.) sites. See Fig. 3 for the daily evolution of temperature at each site.

the same amount of time. Typically, the subsurface does not fully refreeze until late May or the first half of June. The onset of the thawing period may be delayed for up to one month in case of persisting snow cover, although the end of the thawing period rarely shifts as much, as by late summer there is no significant snowfall or snow accumulation.

2.1.3. Tejos site

The Tejos site is located ~2.5 km northwards from the OSM at 5,830 m a.s.l., in a mountain tundra periglacial environment. The site is in a flat area amid thick lava flows, moraine ridges, and rock glacier deposits.

The site is part of a perennial firn-fed outwash plain, with occasional snow and wind-carved boulders without sand accumulations or traces of cryoturbation. The slopes are dominated by solifluction lobes, with huge debris slopes leading to the top of the massif. The specific monitoring location does not show signs of meltwater flooding but a consistent blanket of gravel lag deposits, with the largest grain size out of the three monitoring sites. As at Atacama, the regolith's coarser (>2 mm) fraction is finer at 35 cm depth, with a higher silt fraction around this depth as well. The bulk density of the regolith is the lowest out of all sites: 1.1, 1.3, and 1.0 g/cm^3 at depths of 10, 35, and 60 cm, respectively. The porosity of the sediment is even higher than at Atacama, ranging between 55-67% v/v (Nagy *et al.*, 2019).

At this site, the daily temperature measurements (Table 1) show a persistent presence of ice-bearing permafrost at least since February 2012. Thermal loggers placed near the permafrost table at 60 cm depth are occasionally frozen until mid-February. According to the phase-change model of Nagy *et al.* (2020), the active layer thickens to a maximum of 70-80 cm. At the surface, regolith thawing starts in early November and freezes again in early April. The thawing reaches the bottom of the active layer by the end of February or the beginning of March, *i.e.*, requiring between 100-120 days. The refreezing rate at Tejos is twice as fast as at Atacama. The onset of the thawing period can be delayed by up to a month due to the snow cover effect and its termination shortened to the beginning of March, although transient, refreezing events may occur at any stage of the melting period particularly in the upper 10-20 cm. This delayed thawing occurs when snow does not sublimate following summer snowfalls but rather it melts over several weeks, with meltwater soaking the surface, creating temporary ice cement.

2.2. Determination of subsurface permafrost structures

2.2.1. Freezing and thawing indicators

The likelihood of permafrost occurrence in the three study sites was analyzed by means of surface temperature datasets from 2012-2023 for the Atacama and Tejos sites, and 2014-2023 for the Murray site (Fig. 4 and Table 1). All thermal loggers were located on a horizontal surface, far from any shading topographic feature (see Nagy *et al.*, 2019 for more information on the measurement procedure). The loggers were of the type HOBO Pro v2 (U22-001), with an operation range from -40 to 70 °C, an accuracy of ±0.21 °C from 0 to 50 °C, and a resolution of 0.02 °C at 25 °C.

The thermal exposure was estimated for each site through the freezing/thawing degree days and the Frost number (F^+) (Nelson and Outcalt, 1987; Barry and Gan, 2011, p. 172). The total annual freezing (FDD) and thawing (TDD) days are defined as the cumulative number of days in a year with daily air temperatures below and above 0 °C, respectively. The Frost number is a simplified index for the likelihood of permafrost occurrence and is calculated as follows:

$$F^+ = \frac{\sqrt{\mathrm{FDD}}}{\sqrt{\mathrm{FDD}} + \sqrt{\mathrm{TDD}}} \qquad \text{Eq. 1}$$

These estimates compare the overall magnitude of thermal exposure between sites, such as the n-factor determination (see Klene *et al.*, 2001), and help compare frost exposure and permafrost conditions in periglacial environments (Ran *et al.*, 2015).

Frost numbers can define the occurrence probability of permafrost as follows: continuous ($F^+ \geq 0.67$), discontinuous ($0.67 > F^+ \geq 0.6$), sporadic ($0.6 > F^+ \geq 0.5$), and no ($F^+ < 0.5$) permafrost (Barry and Gan, 2011).

2.2.2. Electrical resistivity tomography

Electrical resistivity tomography (ERT) is a standard geophysical method to investigate subsurface structures and identify their properties. By combining ERT with permafrost occurrence estimates, more confident permafrost thicknesses can be determined (Nagy *et al.*, 2020).

All ERT surveys conducted during this study took place around noon. The data were collected with a 4-point light Lippmann resistivity meter with a distance between electrodes of 10 m for the Murray and Atacama sites and 5 m for the Tejos site. The array employed for the resistivity lecture was dipole-dipole (see Kneisel, 2006) due to a better performance in terms of penetration depth. Four profiles were surveyed, one at Murray (195 m length), two at Atacama (95 and 195 m length), and one at Tejos (145 m length) (Table 2). To process the data and generate the calculated resistivity profiles, the Res2DInv 5.0 inversion software (Loke and Barker, 1996) was used. In all ERT surveys, there were no significant error issues on electrode contact resistance.

3. Results

3.1. Permafrost occurrence

The Frost number estimations were 0.34, 0.53, and 0.72 for the Murray, Atacama, and Tejos sites, respectively. Surface temperature datasets at 10 cm depth evidence frost conditions representative of a permafrost environment at Tejos, a sporadic occurrence at Atacama and no permafrost at Murray. These estimates suggest an altitudinal gradient for mountain permafrost occurrence at the OSM, accounting for a negative control, a fringe area, and a favorable site for frozen grounds by the end of the warm season.

3.2. Geophysical data

Figure 5 presents the electrical resistivity profiles obtained at the three sites. The ERT transect at Murray (Fig. 5A) shows two layers and a half-space separated by two evident resistivity contrasts. First, a ~2-6 m-thick surface layer with low resistivity values (0.2-0.5 kΩm), beneath it, a meter-thick, intermediate layer not parallel to the surface with higher resistivity values (1-7 kΩm) and a half-space with resistivities <5 kΩm below.

At Atacama, the N-S transect (Fig. 5B) evidences a ~3 m-thick surface layer with resistivities ranging between 0.5-2 kΩm. A clear high resistivity layer (15-20 kΩm) appears in the southern half of the profile and thins northwards. In the E-W resistivity profile (Fig. 5C), it is possible to define three different resistivity layers: (i) a shallow, 3 m-thick, low resistivity layer (0.5-2.5 kΩm); (ii) an intermediate, 20 m-thick, high resistivity layer (15-20 kΩm); and (iii) a bottom half-space with resistivities lower than 5 kΩm.

At Tejos, there is a shallow, 2-5 m-thick layer with resistivities below 10 kΩm, that overlies a 20 m-thick domain with resistivity values of up to 100 kΩm. The Tejos site exhibits higher resistivity domains than those observed at the other sites and more contrasting resistivity transitions overall.

4. Discussion

The thermal analysis evidences a transition from mountain desert without permafrost (Murray) to a mountain periglacial zone with ice-rich permafrost (Tejos), where the active layer is assumed to be present above ~5,260 m a.s.l. In fact, at Tejos, the thawing degree days are dramatically lower when compared to Atacama and Murray, even though the percentage of freeze-thaw cycle days does not show this contrast as evidently. This aspect is clearly shown in Figure 4 as well, where temperatures at 60 cm depth remained always below 0 °C at Tejos, indicative of either a permafrost-table top or a thermal transition for ice-phase change.

4.1. Discretization of permafrost structures

The ERT results do not unequivocally confirm an altitudinal gradient from no frozen grounds (Murray)

TABLE 2. LOCATION OF GEOPHYSICAL SURVEY SITES IN THE OJOS DEL SALADO MASSIF.

Sites	Altitude [m a.s.l.]	Latitude	Longitude	ERT profile length [m]
Murray	4,550	26°56′01″ S	68°36′49″ W	195
Atacama	5,260	27°04′32″ S	68°33′51″ W	195 and 95
Tejos	5,830	27°05′14″ S	68°32′17″ W	145

See Figure 3 for map locations.

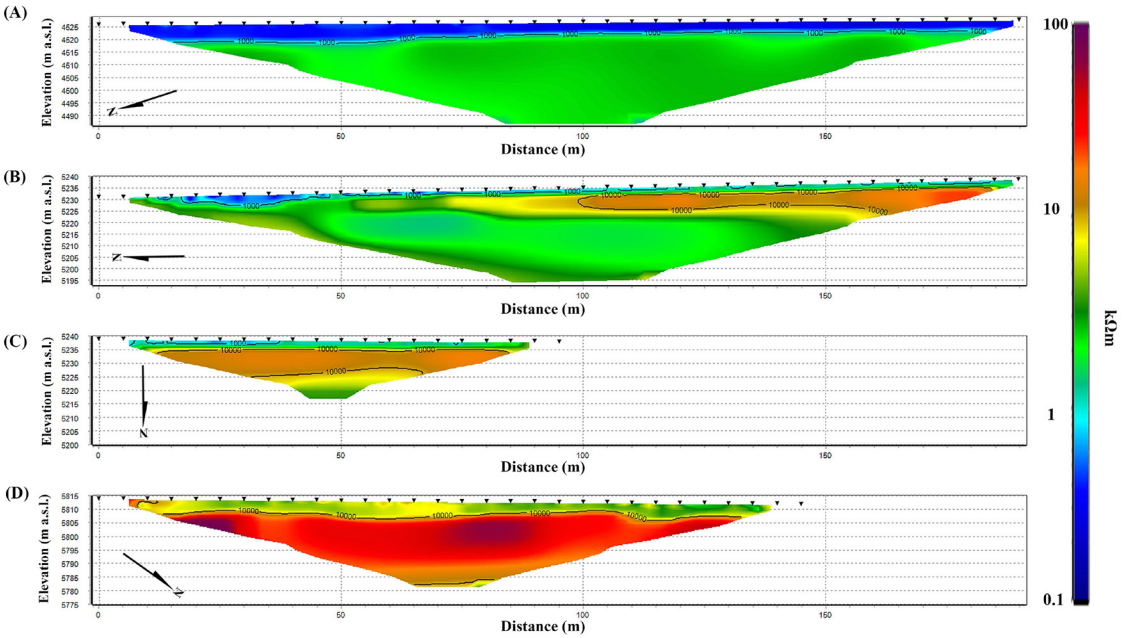

FIG. 5. Electrical resistivity profiles. **A.** Murray, N-S transect. **B.** Atacama, N-S transect. **C.** Atacama, W-E transect. **D.** Tejos, N-S transect. See figure 3 for a location map. Black triangles are 5 m scale for reference, not the electrode spacing. Isocontours are given in Ωm.

up to subsurface values common for permafrost bodies (Tejos). However, there is a consistent resistivity increase at Atacama below 3 m depth, reaching values between 15-20 kΩm. Below 20 m depth, there are important differences in the resistivity values and their spatial extent for all sites. For example, at Murray, there is a large continuous body <5 kΩm, while at Atacama there are lens-like bodies with resistivities of up to 20 kΩm above a less homogeneous <5 kΩm domain. The high-resistive features in the Atacama site thin northwards and longitudinally (Fig. 5C), while at Tejos, in contrast, the predominant subsurface feature is a highly resistive body reaching even 100 kΩm in certain parts.

According to the geological information of the study area (Clavero *et al.*, 2012; Naranjo *et al.*, 2019), the high resistivity values measured at Murray can be indicative of the Laguna Verde ignimbrite. At shallow depths, the low resistivity values could refer to salty alluvial sediments whereas the high-resistivity m-thick body beneath could be a confined aquifer, possibly part of a sedimentary layer just above the ignimbrite. At higher altitudes, ERT data at the Atacama and Tejos sites show the presence of >10 kΩm resistivity structures in the subsurface, possibly lava flows, whose spatial variability can be explained by the phase change of the interstitial water. The ~10 kΩm threshold can particularly be related to the limit between frozen and no frozen material. At the Tejos site, the <5 m-thick, low resistivity shallow body would be indicative of alluvial deposits.

The high resistivity domains imaged particularly at Tejos are consistent with those observed at around 30-31° S in the Argentine Andes (Halla *et al.*, 2021; Villarroel *et al.*, 2022) and at around 28° S in the Chilean Andes (Hilbich *et al.*, 2021; Mathys *et al.*, 2022). These high resistivity values are also consistent with findings in the Alps (Krautblatter and Hauck, 2007; Buckel *et al.*, 2022), establishing unfrozen states below ~10 kΩm and comparable to measured rock resistivity values near 0 ºC (Scandroglio *et al.*, 2021). The bodies imaged in the Alps may be associated with a putative transition layer between the active layer and the permafrost table (Arenson *et al.*, 2022). Therefore, the Tejos high resistivity domains are interpreted as frozen materials with an indeterminate quantity of ice.

By taking together ERT analyses, subsurface frost depths, and Frost numbers, we suggest that the most probable cause for the order-of-magnitude increase in electrical resistivity from Murray to Atacama and Tejos is the increasing presence of frozen ground.

It is also worth noticing that as the ERT survey took place at the end of summer, the high resistivity anomalies detected cannot be snowstorm driven.

4.2. Cryo-hydrogeological implications

As the active layer stores and conducts water (Fig. 2), the thawing period and depth are indicators of a warming environment impacting surface hydrology (Schuur *et al.*, 2015; Walvoord and Kurylyk, 2016). For example, a deeper thawing implies a deepening of flow paths, expanding unconfined aquifers (Sjöberg *et al.*, 2021) and perturbing the background flow field (Wang *et al.*, 2014), therefore enabling transitions into different hydrogeological frameworks (Fig. 2).

The assumption of a continuous transition layer at around 10 kΩm, limiting frozen from unfrozen sediments, implies a consistent frozen body from the shallow surface down to at least 25 m depth as in the case of the Tejos site (Fig. 5D). At Atacama, the same resistivity threshold criterion suggests a lenticular and wedge-like shape for these frozen bodies, with thicknesses below 10 m (Fig. 5B, C). The presence of a consistent, rather homogeneous active layer at Tejos implies that upon surface recharge, the sediment transport yield could accumulate finer grain size above the transition layer. In contrast, the lens-like distribution observed at Atacama could imply a less effective sediment transport with multi-entry points. The potential finding of frozen, lens-like features with distinct salinity (as in deserts) and grain size could represent moderately conductive anomalies along resistive profiles, or a different case with partially frozen sediments (Campbell *et al.*, 2021) with resistivities portraying the ice-phase change transition.

In arid areas, high surface salinity results from former water bodies affected by cryogenic desiccation and wind activity (Kereszturi *et al.*, 2022). A ground with high salinity will have a low resistivity when imaged by ERT techniques, which suggests that some of the low resistivities observed in the study area would be indicative of high saline conditions in the shallow ground. Ground surface salinity measured at Atacama (78.1 µS/cm) and Tejos (224 µS/cm) could represent the effect of in-situ salinity concentration (Aszalós *et al.*, 2020).

In volcanic areas, preferential pathways for fluid circulation exist due to a high hydraulic conductivity gradient between structures (Vittecoq *et al.*, 2019). In addition, geothermal gradient studies in volcanic areas require basic thermal modeling to contrast each site's structural and geophysical data (Nagy *et al.*, 2020). Hence, despite considering a high geothermal gradient as the bottom boundary condition, a bottom-up thawing cannot be longer sustained based on the ERT data, as results are highly indicative of the presence of m-thick frozen structures in the subsurface.

4.3. Limitations and research opportunities

Geophysical surveys around poorly monitored areas without boreholes or previous geophysical assessments are challenging, particularly in high-altitude, remote areas. As such, uncertainties emerge and need to be identified and quantified accordingly. The use of analog hydrogeological settings can be a useful approach. Analogs to the case study presented here can be found in Martian interpretations (Michalski *et al.*, 2013), where volcanically outgassed water would have been locked as taliks, the water equivalent being periodically mobilized, recharging the subsurface through basal thawing.

One limitation of the ERT method is the lack of statistical calibration for the inferred subsurface materials. This deals with both the pore-size-related complexity in saturation estimation and the reactance of either liquid water or ice, as both materials differ in their dielectric properties. For instance, when working over resistive material, the interpreted electrical resistance should account for the ubiquitous presence of weakly conductive and nonconductive pores in rocks and sediments (Zhu *et al.*, 2023). In permafrost areas, these bodies could behave either as Archie or non-Archie rocks depending on their clay content and temperature. Furthermore, in the case of interstitial water/ice, concentration and uniformity determinations need to be calibrated if water equivalent data is required.

Another source of uncertainty is the possible phase transitions from thawed to frozen ground in fine-grained and saline sediments (O'Neill *et al.*, 2019). This can be addressed by identifying the resistivity values along the transition layers that surround highly resistive bodies, allowing more precise geometrical constraints and water-equivalent quantification. By taking this approach, it may be possible to track permafrost degradation in terms of pore water equivalent in larger areas, therefore providing more applied insights for upscaling the effects of climate change on mountainous environments.

Groundwater flow modeling in permafrost settings often lacks robust hydrogeological field data (Kurylyk and Walvoord, 2021, p. 514), so the assessment presented here aims to strengthen the physical foundations for high Andean environments by providing geocryological data for subsequent evaluations of critical groundwater thresholds. Lastly, from a bottom-up perspective, potential recharge impacts on vadose zone infiltration remained unaccounted for. It is therefore essential to consider that, when dealing with volcanic settings, the computation of geothermal gradients should consider: (i) temperature boreholes deeper than 20 m; (ii) an indirect characterization of temperatures from ERT profiles against resistivity curves of thawing sediments; and (iii) hydrochemical analyses as a proxy of water subsurface origin with temperature variability as a proxy of depth. Overall, direct temperature and/or geotechnical data are required to constrain the inversion models and reduce the uncertainty in the derived results.

5. Conclusions

This study confirms a permafrost altitudinal gradient between 4,550-5,830 m a.s.l. at the Ojos del Salado massif in the dry Andes by integrating electrical resistivity surveys and decade-long ground surface temperature datasets.

At sites where the temperature data favors permafrost occurrence, the resistivity surveys reveal consistent differences attesting to high resistivities associated with permafrost thicknesses of about 25 m in the coldest and highest altitude site (Tejos). Abrupt resistivity gradients and well-defined ~10 kΩm resistivity bodies at Atacama and Tejos are indicative of possible transition layers. These results are consistent with previous studies on active rock glaciers in the Alps and the Andes and confirm the presence of frozen ground layers at the Ojos del Salado massif.

This study has implications for better understanding groundwater recharge, surface water dynamics, and the overall response of hydrological systems to climate change in high-altitude, cold-dry settings. Despite their limitations, geophysical surveys afford research opportunities for cold, remote sites. Further integration of field data and improved modeling approaches will be crucial for evaluating groundwater dynamics, groundwater-surface water partition and their effects on streamflow, as well as future tipping points of stagnation, upwelling events, flow path variation, and novel hydrological connections in these sensitive environments.

Acknowledgments

Author contributions. SRP and SL organized the first manuscript drafts, fieldwork, and data analysis. GY contributed to geophysical formal analysis and interpretation. SRP, SL, and FS analyzed and interpreted thermal data and worked on the final paper focus, structure, and organization. SRP, EM, and EB performed fieldwork. BN integrated field temperature data and participated in fieldwork at the Atacama and Tejos sites. This work was supported by Beca Postdoctorado Escuela de Ingeniería, Pontificia Universidad Católica de Chile, and the ANID-FONDECYT Postdoctorado Nacional Folio 3230723. The authors also acknowledge the Laboratorio de Evaluación y Control de Calidad del Agua, DIHA-PUC, Chile. All authors reviewed and actively commented on the manuscript. Alfonso Fernández and the Editor helped reviewing this manuscript.

References

Arenson, L.U.; Harrington, J.S.; Koenig, C.E.M.; Wainstein, P.A. 2022. Mountain permafrost hydrology-a practical review following studies from the Andes. Geosciences 12 (2): 48. https://doi.org/10.3390/geosciences12020048

Aszalós, J.M.; Szabó, A.; Megyes, M.; Anda, D.; Nagy, B.; Borsodi, A.K. 2020. Bacterial diversity of a high-altitude permafrost thaw pond located on Ojos del Salado (Dry Andes, Altiplano-Atacama Region). Astrobiology 20 (6): 754-765. https://doi.org/10.1089/ast.2018.2012

Barry, R.; Gan, T.Y. 2011. The global cryosphere: past, present and future. Cambridge University Press: 472 p. https://doi.org/10.1017/CBO9780511977947

Bartsch, A.; Grosse, G.; Kääb, A.; Westermann, S.; Strozzi, T.; Wiesmann, A.; Duguay, C.; Seifert, F.M.; Obu, J.; Goler, R. 2016. GlobPermafrost-how space-based Earth observation supports understanding of permafrost. *In* Living Planet Symposium, Proceedings, ESA SP: 740 p. Prague.

Bense, V.F.; Ferguson, G.; Kooi, H. 2009. Evolution of shallow groundwater flow systems in areas of degrading permafrost. Geophysical Research Letters 36 (22): L22401. https://doi.org/10.1029/2009GL039225

Bense, V.F.; Person, M.A. 2008. Transient hydrodynamics within intercratonic sedimentary basins during glacial cycles. Journal of Geophysical Research, Earth Surface 113 (F4): F04005. https://doi.org/10.1029/2007JF000969

Bethke, C.M.; Johnson, T.M. 2002. Paradox of groundwater age. Geology 30 (2): 107-110. https://doi.org/10.1130/0091-7613(2002)030<0107:POGA>2.0.CO;2

Bethke, C.M.; Johnson, T.M. 2008. Groundwater age and groundwater age dating. Annual Review of Earth and Planetary Sciences 36: 121-152. https://doi.org/10.1146/annurev.earth.36.031207.124210

Bishop, K.; Buffam, I.; Erlandsson, M.; Folster, J.; Laudon, H.; Seibert, J.; Temnerud, J. 2008. Aqua Incognita: the unknown headwaters. Hydrological Processes 22 (8): 1239-1242. https://doi.org/10.1002/hyp.7049

Buckel, J.; Mudler, J.; Gardeweg, R.; Hauck, C.; Hilbich, C.; Frauenfelder, R.; Kneisel, C.; Buchelt, S.; Blöthe, J.H.; Hördt, A. 2022. Identifying mountain permafrost degradation by repeating historical electrical resistivity tomography (ERT) measurements. The Cryosphere 17 (7): 2919-2940. https://doi.org/10.5194/tc-17-2919-2023

Campbell, S.W.; Briggs, M.; Roy, S.G.; Douglas, T.A.; Saari, S. 2021. Ground-penetrating radar, electromagnetic induction, terrain, and vegetation observations coupled with machine learning to map permafrost distribution at Twelvemile Lake, Alaska. Permafrost and Periglacial Processes 32 (3): 407-426. https://doi.org/10.1002/ppp.2100

Clavero, J.; Mpodozis, C.; Gardeweg, M.; Valenzuela, M. 2012. Geología de las áreas Laguna Wheelwright y Paso San Francisco, Región de Atacama. Servicio Nacional de Geología y Minería, Carta Geológica de Chile, Serie Geología Básica 139-140: 32 p. Santiago.

Cochand, M.; Molson, J.; Barth, J.A.C.; van Geldern, R.; Lemieux, J.M.; Fortier, R.; Therrien, R. 2020. Rapid groundwater recharge dynamics determined from hydrogeochemical and isotope data in a small permafrost watershed near Umiujaq (Nunavik, Canada). Hydrogeology Journal 28: 853-858. https://doi.org/10.1007/s10040-020-02109-x

Cuthbert, M.O.; Gleeson, T.; Moosdorf, N.; Befus, K.M.; Schneider, A.; Hartmann, J.; Lehner, B. 2019. Global patterns and dynamics of climate-groundwater interactions. Nature Climate Change 9 (2): 137-141.

Evans, S.G.; Ge, S. 2017. Contrasting hydrogeologic responses to warming in permafrost and seasonally frozen ground hillslopes. Geophysical Research Letters 44 (4): 1803-1813. https://doi.org/10.1002/2016GL072009

Gleeson, T.; Cuthbert, M.; Ferguson, G.; Perrone, D. 2020. Global groundwater sustainability, resources, and systems in the Anthropocene. Annual review of earth and planetary sciences 48 (1): 431-463.

Halla, C.; Blöthe, J.H.; Tapia Baldis, C.; Trombotto Liaudat, D.; Hilbich, C.; Hauck, C.; Schrott, L. 2021. Ice content and interannual water storage changes of an active rock glacier in the dry Andes of Argentina. The Cryosphere 15 (2): 1187-1213. https://doi.org/10.5194/tc-15-1187-2021

Hammond, J.C.; Harpold, A.A.; Weiss, S.; Kampf, S.K. 2019. Partitioning snowmelt and rainfall in the critical zone: effects of climate type and soil properties. Hydrology and Earth System Sciences 23 (9): 3553-3570. https://doi.org/10.5194/hess-23-3553-2019

Hilbich, C.; Hauck, C.; Mollaret, C.; Wainstein, P.; Arenson, L.U. 2021. Towards accurate quantification of ice content in permafrost of the Central Andes, Part 1: geophysics-based estimates from three different regions. The Cryosphere 16 (5): 1845-1872. https://doi.org/10.5194/tc-16-1845-2022

Houston, J.; Hart, D. 2004. Theoretical head decay in closed basin aquifers: an insight into fossil groundwater and recharge events in the Andes of northern Chile. Quarterly Journal of Engineering Geology and Hydrogeology 37 (2): 131-139. https://doi.org/10.1144/1470-9236/04-007

Jasechko, S.; Perrone, D. 2021. Global groundwater wells at risk of running dry. Science 372 (6540): 418-421. https://doi.org/10.1126/science.abc2755

Jin, X.-Y.; Jin, H.-J.; Iwahana, G.; Marchenko, S.S.; Luo, D.-L.; Li, X.-Y.; Liang, S.-H. 2021. Impacts of climate-induced permafrost degradation on vegetation: A review. Advances in Climate Change Research 12 (1): 29-47. https://doi.org/10.1016/j.accre.2020.07.002

Jorgenson, M.T.; Racine, C.H.; Walters, J.C.; Osterkamp, T.E. 2001. Permafrost degradation and ecological changes associated with a warming climate in central Alaska. Climatic Change 48: 551-579. https://doi.org/10.1023/A:1005667424292

Kereszturi, A.; Aszalós, J.; Heiling, Zs.; Ignéczi, A.; Kapui, Zs.; Király, Cs.; Leél-Őssy, Sz.; Szalai, Z.; Nemerkényi, Zs.; Pál; B.; Skultéti, A.; Nagy, B. 2022. Wind-snow interactions at the Ojos del Salado region as a potential Mars analogue site in the Altiplano-Atacama desert region. Icarus 378. https://doi.org/10.1016/j.icarus.2022.114941

Klene, A.E.; Nelson, F.E.; Shiklomanov, N.I.; Hinkel, K.M. 2001. The n-factor in natural landscapes: variability of air and soil-surface temperatures, Kuparuk River Basin, Alaska, USA. Arctic, Antarctic, and Alpine Research 33 (2): 140-148. https://doi.org/10.1080/15230430.2001.12003416

Kneisel, C. 2006. Assessment of subsurface lithology in mountain environments using 2D resistivity imaging. Geomorphology 80 (1-2): 32-44. https://doi.org/10.1016/j.geomorph.2005.09.012

Krautblatter, M.; Hauck, C. 2007. Electrical resistivity tomography monitoring of permafrost in solid rock

walls. Journal of Geophysical Research, Earth Surface 112 (F2): F02S20. https://doi.org/10.1029/2006JF000546

Kurylyk, B.L.; Walvoord, M.A. 2021. Permafrost hydrogeology. *In* Arctic hydrology, permafrost and ecosystems (Yang, D.; Kane, D.L.; editors). Springer: 493-523. Cham. https://doi.org/10.1007/978-3-030-50930-9_17

Leray, S.; de Dreuzy, J.-R.; Bour, O.; Bresciani, E. 2013. Numerical modeling of the productivity of vertical to shallowly dipping fractured zones in crystalline rocks. Journal of Hydrology 481: 64-75. https://doi.org/10.1016/j.jhydrol.2012.12.014

Liao, C.; Zhuang, Q. 2017. Quantifying the role of permafrost distribution in groundwater and surface water interactions using a three-dimensional hydrological model. Arctic, Antarctic, and Alpine Research 49 (1): 81-100. https://doi.org/10.1657/AAAR0016-022

Loke, M.H.; Barker, R.D. 1996. Rapid least-squares inversion of apparent resistivity pseudosections by a quasi-Newton method. Geophysical Prospecting 44 (1): 131-152. https://doi.org/10.1111/j.1365-2478.1996.tb00142.x

IPCC (Intergovernmental Panel on Climate Change) 2023. Summary for Policymakers. *In* Climate Change 2023: Synthesis Report. Contribution of Working Groups I, II and III to the Sixth Assessment Report of the Intergovernmental Panel on Climate Change (Core Writing Team; Lee, H.; Romero,J.; editor). Intergovernmental Panel on Climate Change: 1-34. Geneva. https://doi.org/10.59327/IPCC/AR6-9789291691647.001

Mathys, T.; Hilbich, C.; Arenson, L.U.; Wainstein, P.A.; Hauck, C. 2022. Towards accurate quantification of ice content in permafrost of the Central Andes-Part 2: an upscaling strategy of geophysical measurements to the catchment scale at two study sites. The Cryosphere 16 (6): 2595-2615. https://doi.org/10.5194/tc-16-2595-2022

Meju, M.A. 2002. Geoelectromagnetic exploration for natural resources: models, case studies and challenges. Surveys in Geophysics 23: 133-206. https://doi.org/10.1023/A:1015052419222

Michalski, J.R.; Cuadros, J.; Niles, P.B.; Parnell, J.; Deanne Rogers, A.; Wright, S.P. 2013. Groundwater activity on Mars and implications for a deep biosphere. Nature Geoscience 6: 133-138. https://doi.org/10.1038/ngeo1706

Musselman, K.N.; Clark, M.P.; Liu, C.; Ikeda, K.; Rasmussen, R. 2017. Slower snowmelt in a warmer world. Nature Climate Change 7: 214-219. https://doi.org/10.1038/nclimate3225

Nagy, B.; Ignéczi, Á.; Kovács, J.; Szalai, Z.; Mari, L. 2019. Shallow ground temperature measurements on the highest volcano on Earth, Mt. Ojos del Salado, Arid Andes, Chile. Permafrost and Periglacial Processes 30(1): 3-18. https://doi.org/10.1002/ppp.1989

Nagy, B.; Kovács, J.; Ignéczi, Á.; Beleznai, S.; Mari, L.; Kereszturi, Á.; Szalai, Z. 2020. The thermal behavior of ice-bearing ground: the highest cold, dry desert on Earth as an analog for conditions on Mars, at Ojos del Salado, Puna de Atacama-Altiplano region. Astrobiology 20 (6): 701-722. https://doi.org/10.1089/ast.2018.2021

Nagy, B.; Ignéczi, Á.; Kovács-Székely, I.; Pereira, S.R.; Mihajlik, G.; Felkai, P.; Mari, L. 2023. The challenges of commercial mountaineering on the highest Volcanic Seven Summit, the Ojos del Salado. Hungarian Geographical Bulletin 72 (1): 23-40. https://doi.org/10.15201/hungeobull.72.1.2

Naranjo, J.A.; Hevia, F.; Arcos, R.; Polanco, E. 2019. Geología de las áreas Nevado Ojos del Salado y Cerro El Fraile, Región de Atacama. Servicio Nacional de Geología y Minería, Carta Geológica de Chile, Serie Geología Básica 147: 37 p. Santiago.

Nelson, F.E.; Outcalt, S.I. 1987. A computational method for prediction and regionalization of permafrost. Arctic and Alpine Research 19 (3): 279-288. https://doi.org/10.1080/00040851.1987.12002602

Obu, J.; Westermann, S.; Kääb, A.; Bartsch, A. 2019. Ground Temperature Map, 2000-2016, Andes, New Zealand and East African Plateau Permafrost (dataset). University of Oslo, PANGAEA. https://doi.org/10.1594/PANGAEA.905512

O'Neill, H.B.; Wolfe, S.A.; Duchesne, C. 2019. New ground ice maps for Canada using a paleogeographic modelling approach. The Cryosphere 13 (3): 753-773. https://doi.org/10.5194/tc-13-753-2019

Perrone, D.; Jasechko, S. 2019. Deeper well drilling an unsustainable stopgap to groundwater depletion. Nature Sustainability 2: 773-782. https://doi.org/10.1038/s41893-019-0325-z

Ran, Y.; Li, X.; Jin, R.; Guo, J. 2015. Remote sensing of the mean annual surface temperature and surface frost number for mapping permafrost in China. Arctic, Antarctic, and Alpine Research 47 (2): 255-265. https://doi.org/10.1657/AAAR00C-13-306

Ravenscroft, P.; Burgess, W.G.; Ahmed, K.M.; Burren, M.; Perrin, J. 2005. Arsenic in groundwater of the Bengal Basin, Bangladesh: distribution, field relations, and hydrogeological setting. Hydrogeology Journal 13: 727-751. https://doi.org/10.1007/s10040-003-0314-0

Scandroglio, R.; Draebing, D.; Offer, M.; Krautblatter, M. 2021. 4D quantification of alpine permafrost degradation in steep rock walls using a laboratory-calibrated electrical resistivity tomography approach. Near Surface Geophysics 19 (2): 241-260. https://doi.org/10.1002/nsg.12149

Schuur, E.A.G.; McGuire, A.D.; Schädel, C.; Grosse, G.; Harden, J.W.; Hayes, D.J.; Hugelius, G.; Koven, C.D.; Kuhry, P.; Lawrence, D.M.; Natali, S.M.; Olefeldt, D.; Romanovsky, V.E.; Schaefer, K.; Turetsky, M.R.; Treat, C.C.; Vonk, J.E. 2015. Climate change and the permafrost carbon feedback. Nature 520: 171-179. https://doi.org/10.1038/nature14338

Sjöberg, Y.; Jan, A.; Painter, S.L.; Coon, E.T.; Carey, M.P.; O'Donnell, J.A.; Koch, J.C. 2021. Permafrost promotes shallow groundwater flow and warmer headwater streams. Water Resources Research 57 (2): e2020WR027463. https://doi.org/10.1029/2020WR027463

Somers, L.D.; McKenzie, J.M. 2020. A review of groundwater in high mountain environments. WIREs Water 7 (6): e1475. https://doi.org/10.1002/wat2.1475

Uhlemann, S.; Dafflon, B.; Peterson, J.; Ulrich, C.; Shirley, I.; Michail, S.; Hubbard, S.S. 2021. Geophysical monitoring shows that spatial heterogeneity in thermohydrological dynamics reshapes a transitional permafrost system. Geophysical Research Letters 48 (6): e2020GL091149. https://doi.org/10.1029/2020GL091149

Villarroel, C.D.; Ortiz, D.A.; Forte, A.P.; Tamburini Beliveau, G.; Ponce, D.; Imhof, A.; López, A. 2022. Internal structure of a large, complex rock glacier and its significance in hydrological and dynamic behavior: A case study in the semi-arid Andes of Argentina. Permafrost and Periglacial Processes 33: 78-95. https://doi.org/10.1002/ppp.2132

Vittecoq, B.; Reninger, P.-A.; Lacquement, F.; Martelet, G.; Violette, S. 2019. Hydrogeological conceptual model of andesitic watersheds revealed by high-resolution heliborne geophysics. Hydrology and Earth System Sciences 23 (5): 2321-2338. https://doi.org/10.5194/hess-23-2321-2019

Walvoord, M.A.; Kurylyk, B.L. 2016. Hydrologic impacts of thawing permafrost-a review. Vadose Zone Journal 15 (6): 1-20. https://doi.org/10.2136/vzj2016.01.0010

Wang, J.-Z.; Jiang, X.-W.; Wan, L.; Wang, X.-S.; Li, H. 2014. An analytical study on groundwater flow in drainage basins with horizontal wells. Hydrogeology Journal 22: 1625-1638. https://doi.org/10.1007/s10040-014-1146-9

Zhu, L.; Wu, S.; Zhang, C.; Misra, S.; Zhou, X.; Cai, J. 2023. Characterization of pore electrical conductivity in porous media by weakly conductive and nonconductive pores. Surveys in Geophysics 44: 877-923. https://doi.org/10.1007/s10712-022-09761-w

Zinn, B.A.; Konikow, L.F. 2007. Potential effects of regional pumpage on groundwater age distribution. Water Resources Research 43 (6): W06418. https://doi.org/10.1029/2006WR004865

Manuscript received: April 15, 2024; revised/accepted: December 05, 2024; available online: January 31, 2025.

Journal of Hydrology 653 (2025) 132741

Contents lists available at ScienceDirect

Journal of Hydrology

journal homepage: www.elsevier.com/locate/jhydrol

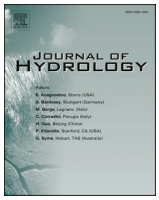

Surface hydrology on the highest volcano of the high Dry Andes, the Ojos del Salado; interannual fluctuations and moisture sources

Balázs Nagy [a], Sebastián Ruiz-Pereira [b,c], Ádám Ignéczi [d,*], József Kovács [e], Kaveh Ghahraman [a], Gábor Mihajlik [f], Marianna Túri [g], Zoltán Kern [h]

[a] Department of Physical Geography, Eötvös Loránd University, Budapest, Hungary
[b] Escuela de Ingeniería, Pontificia Universidad Católica de Chile, Santiago, Chile
[c] PermaChile Network, Santiago, Chile
[d] School of Geographical Sciences, University of Bristol, Bristol, UK
[e] Department of Physical and Applied Geology, Eötvös Loránd University, Budapest, Hungary
[f] Department of Atomic Physics, Budapest University of Technology and Economics, Budapest, Hungary
[g] Isotope Climatology and Environmental Research Centre, Institute for Nuclear Research, Eötvös Loránd Research Network, Debrecen, Hungary
[h] Institute for Geological and Geochemical Research, Research Centre for Astronomy and Earth Sciences, Eötvös Loránd Research Network, Budapest, Hungary

ARTICLE INFO

This manuscript was handled by Editor-in-Chief, with the assistance of Francesco Avanzi, Associate Editor

Keywords:
Andes
Permafrost
Hydrology
Tritium
Stable isotope

ABSTRACT

The Atacama Plateau in the Central Andes (28–22°S) is characterised by a dry and cold periglacial tundra due to the high altitude, low precipitation, and high evaporation. Endogenous freshwater sources – e.g.: seasonal streams and lakes, subsurface reservoirs, surface snow/ice patches – are available, though they are highly sensitive to climatic changes. The near surface hydrological network is highly modified by the distribution and seasonal evolution of perennial frozen ground, i.e. permafrost, which is also expected to change in the future. The interplay between permafrost and hydrology, especially in relation to future climate change, is poorly explored. To address this issue, we carry out long-term ground temperature measurement and modelling, snow coverage survey, tritium- and stable isotope analysis of surface waters on the Ojos del Salado Massif, which is representative of high altitude mountains on the Atacama Plateau. According to our results, a highly transient surface hydrological network – lakes, springs and streams – forms during each summer where permafrost is widespread and ground thawing (i.e. active layer) is present (~4900–6500 m a.s.l.). In this system, the water is of meteoric origin and relatively young (<10 years). The development of the network is strongly influenced by the active layer, which plays a crucial role in storing, seeping, and discharging groundwater. However, future permafrost degradation is expected to reduce the seasonal presence of shallow water, and hence, modify groundwater recharge patterns.

1. Introduction

Mountains could be considered freshwater reservoirs for lowlands (Viviroli & Weingartner, 2008) with major recharge from the cryosphere (Barnett et al., 2005). However, throughout the Central and Southern Andes, atmospheric warming and precipitation loss is expected to significantly reduce snow cover by 2100 (Boisier et al., 2018; Bozkurt et al., 2018), thereby accelerating glacier and ice bearing permafrost retreat (Baraer et al., 2012). Thus recharge at high elevations and consequently water supply in lowlands (Cheng & Jin, 2013; Oliva & Fritz, 2018) is also expected to decrease in the region, significantly deteriorating water security (Boisier et al., 2018; Bozkurt et al., 2018). Current trends corroborate these projections, e.g. annual snow cover persistence declined by about 2–5 days between 2000–2016 in the Southern Andes (29–39° S) (Saavedra et al., 2018). This shortage of mountain snow has already caused an extended, severe drought that is unprecedented in the hydrological and climatological records of this region (Masiokas et al., 2020).

On the Atacama Plateau (Puna de Atacama) in the Central Andes (between 28 and 22°S) dry and cold periglacial tundra conditions are predominant due to the high altitude (> 5000 m a.s.l.), low precipitation, and high evaporation (Lobos-Roco et al., 2021). Despite the arid/hyperarid periglacial environment, endogenous freshwater sources such as surface streams and surface/subsurface reservoirs are available

* Corresponding author.
E-mail address: a.igneczi@bristol.ac.uk (Á. Ignéczi).

https://doi.org/10.1016/j.jhydrol.2025.132741
Received 14 March 2024; Received in revised form 28 November 2024; Accepted 12 January 2025
Available online 26 January 2025

(Grosjean et al., 1995; Nicholson, 1998). However, these water sources are highly sensitive to the expected future decline in precipitation across the Dry Andes (Bozkurt et al., 2018) that will diminish recharge in the preferential infiltration zones (Carroll et al., 2019; Wu et al., 2020) and exacerbate future droughts (Alvarez-Garreton et al., 2021). Furthermore, the degradation of permafrost and subsurface ice in a warming climate (Masson-Delmotte et al., 2021) is also expected to modify infiltration patterns and snowmelt partitioning (Hammond et al., 2019); groundwater pathways, flux, and confinement (Cochand et al., 2020); and groundwater discharge to surface streams (Somers & McKenzie, 2020).

Hence, interstitial ice thaw within the arid periglacial zone of the Dry Andes – e.g. the Ojos del Salado near the latitude of 27°S (Obu et al., 2019, Nagy et al., 2019) – due to future warming and drying will have direct implications for aquifer recharge and also for the water budget of the wider region including nearby lowlands. Despite, the expected increase in the role of permafrost – and its degradation – in the hydrological system of the Dry Andes, and other regions with similar conditions, only limited research is available (Arenson et al., 2022). To address this shortcoming, we deploy a wide variety of remote, field and numerical methods – including long-term ground temperature measurement and modelling, satellite remote sensing of snow coverage, radioactive and stable isotope analysis of water samples – on the Ojos del Salado to gain a comprehensive view of the surface and shallow subsurface hydrological system of the mountain. Based on these insights, we also develop a conceptual model of this system, which is directly applicable to the numerous other high altitude massifs of the Dry Andes, and also to similar high-altitude cold and dry tundra environments.

2. Study site

Several major massifs rising above 6000 m a.s.l. – mostly dormant and inactive volcanoes – can be found along the 1000 km long Dry Andes (part of the Central Andes), and also within the even more arid Andean Dry Diagonal (between 27° and 30°S). The highest massifs of the Andean Dry Diagonal have a topographic prominence of about 2000–2500 m from the surrounding Puna Plateau (Fig. 1). Their climate is extremely arid and cold, with precipitation dominated by winter snow which usually forms a thin cover that is present for only a few weeks due to strong sublimation (Kull et al., 2002). Thus active glaciers are arguably absent, though ground ice (i.e. ice bearing permafrost) can be found above 5000 m a.s.l. (Gjorup et al., 2019). Due to the presence of this subsurface ice deposits/reservoirs, these cold high-altitude deserts could be considered the frozen water towers of the Dry Andes.

The highest of these peaks is the Ojos del Salado (6893 m a.s.l., 27°07′34″S 68°32′26″W), the prominent peak of the corresponding Ojos del Salado massif (OSM) which also includes the immediate vicinity/foreground of the volcano (Figs. 1, 2). The OSM is a representative example of this chain of volcanic giants. Measurements from the foreground of the OSM – near the Laguna Verde Station at 4914 m a.sl. (Figs. 1, 2) – between 2012 and 2015 indicate extremely low annual mean precipitation (181 ± 25.5 mm). Furthermore, only two major

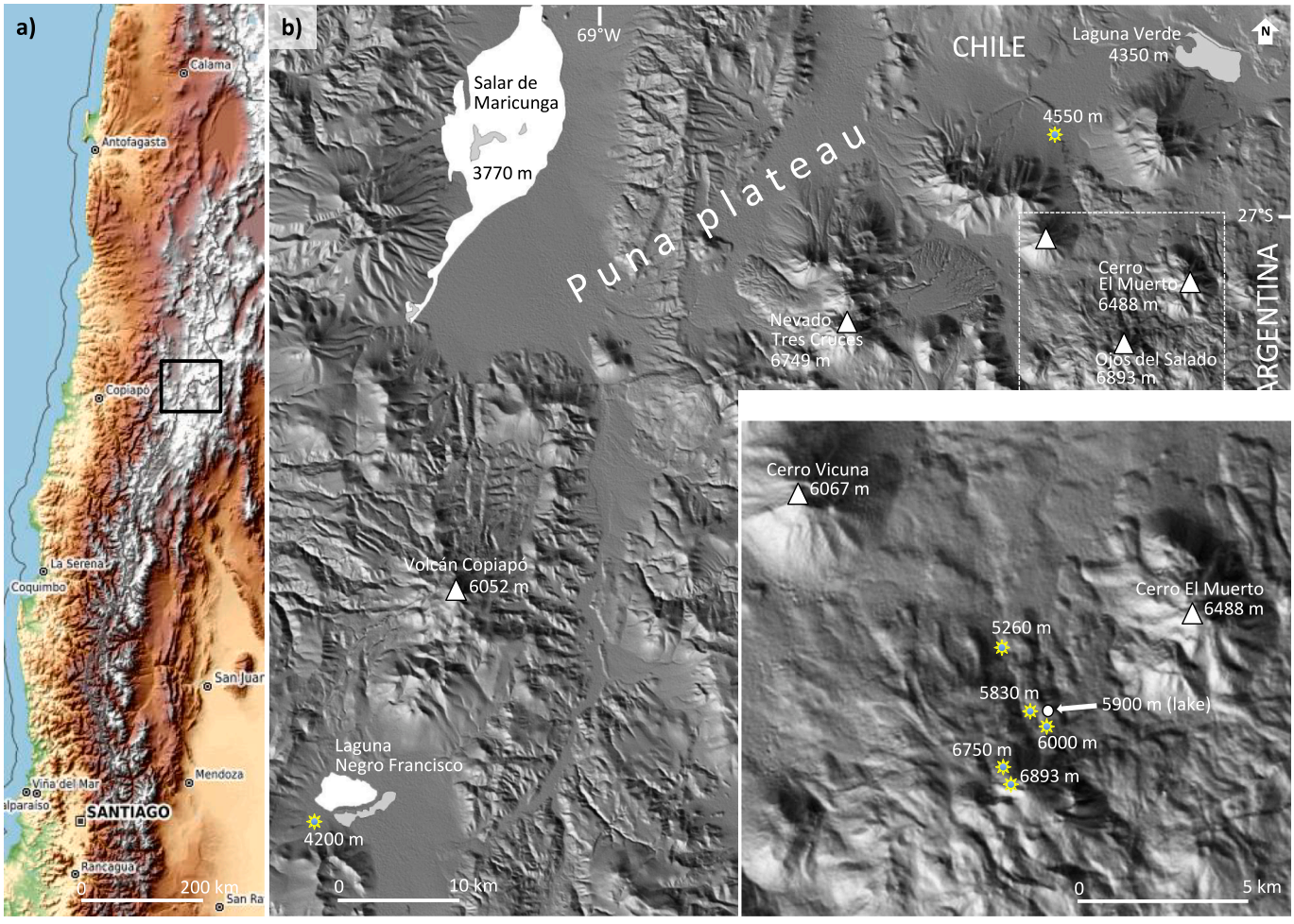

Fig. 1. Location of the Ojos del Salado Massif (OSM) on the Puna de Atacama. Stars indicate the sites of the ground temperature monitoring system.

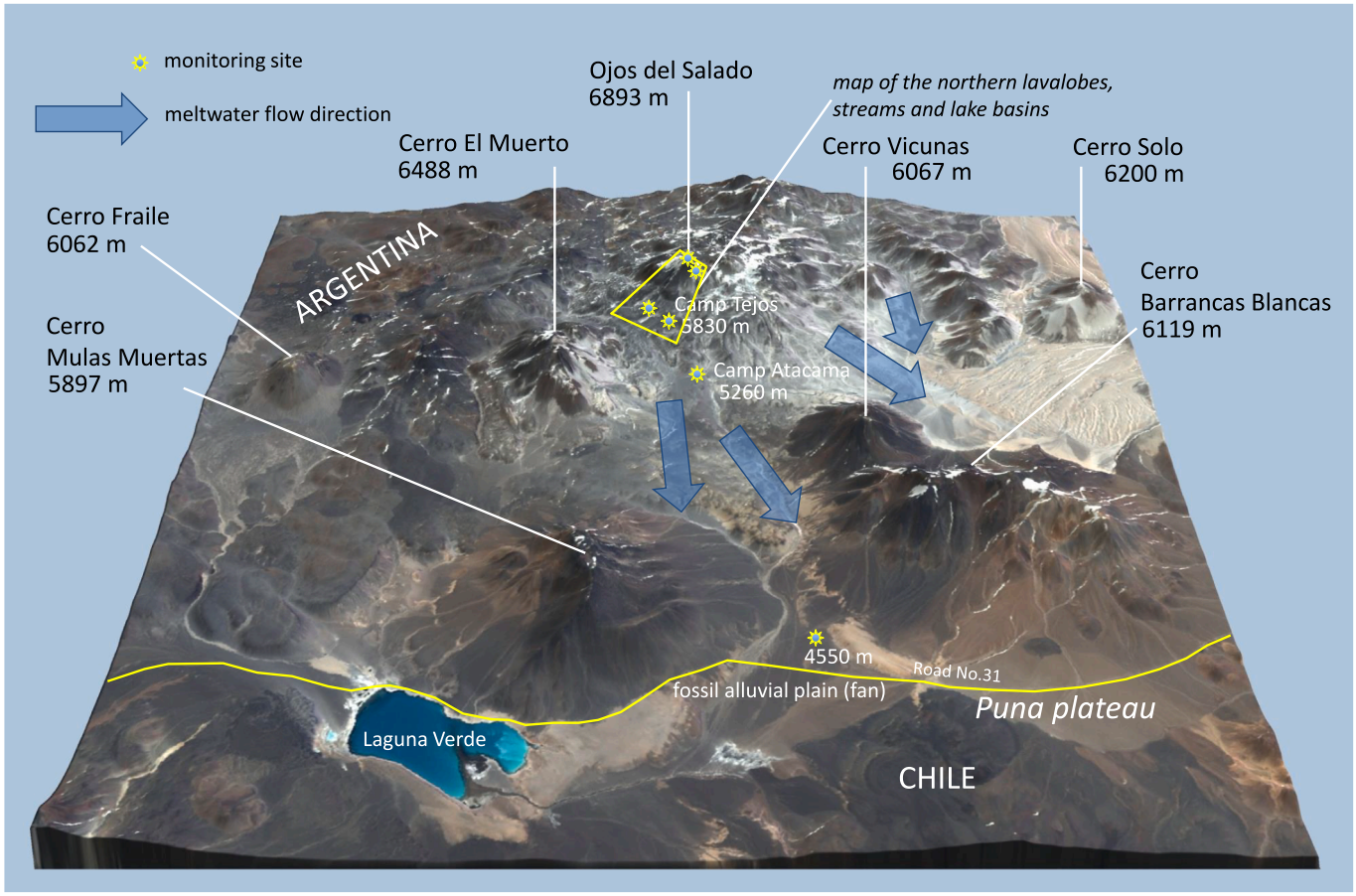

Fig. 2. The Ojos del Salado Massif, viewed from the North. Major peaks within the OSM, our ground temperature monitoring sites (stars), and key meltwater flow directions are indicated.

snow events were detected in the same period: one in 2012 lasting ~ 5 days with a maximum snow depth of 62 mm, and another in 2015 lasting ~ 32 days with a maximum snow depth of 243 mm (DGA-Arcadis, 2015; Enguita, 2016). Accordingly, the presence of surface ice is very limited as the climatic snowline (~7000 m a.s.l.) is estimated to be just above the Ojos del Salado summit (Houston and Hartley, 2003). However, permafrost and ground ice has been detected above 5000–5500 m a.s.l. on the OSM (Nagy et al., 2019). Surface freshwater such as small and shallow ponds (Aszalós et al. 2016, Nagy et al., 2019, 2020), and short streams (Kereszturi et al., 2022) has also been reported from the OSM recently, though only from high elevations (above ~ 5500–5800 m).

Larger, saline lakes – e.g. the Lagune Verde with a corresponding saturated aquifer of 128.7 km2 (Vargas Paysen, 2013) – located in the lower foreground (below ~ 4500 m a.s.l.) of the OSM are well-known and studied. These saline lakes are fed predominantly by warm (up to 36 °C) saline springs and considered to be permanent. However, the temporal persistence, water sources, and hydrological connectivity of high elevation surface ponds and streams on the OSM are largely unknown (Aszalós et al. 2016, 2020; Nagy et al. 2020). Thus, we investigate these features on the northern side of the OSM, where we have established a shallow ground temperature monitoring network in 2012 "from-toe-to-top" covering the elevational range of 4550–6893 m a.s.l. (Fig. 1, Fig. 2). We primarily focus on the vicinity of Camp Atacama (27°04′32″S, 68°33′51″W, 5260 m a.s.l.) and Camp Tejos (27°05′14″S, 68°32′17″W, 5830 m a.s.l.) – covering the elevational range of about 5200–6000 m a.s.l. (Fig. 2) – where permafrost is widespread and summer melting is significant, thus conditions are conducive for the formation of a surface hydrological network (Nagy et al., 2019).

3. Methods

3.1. Ground temperature measurements

Ground thermal regimes, permafrost distribution, and active layer dynamics have been investigated on the OSM since 2012 (Nagy et al., 2019) using our monitoring network (Figs. 1, 2). In this study, two sites were selected from our network on the northern side of the OSM: Camp Atacama (5260 m a.s.l.) and Camp Tejos (5830 m a.s.l.) (Fig. 2). Hourly ground temperatures at shallow depths (10–60 cm) – capturing the active layer – are measured by HOBO Pro v2 temperature loggers (operation range: −40 °C to 70 °C, accuracy: ±0.21 °C) at these sites (Nagy et al., 2019). The study period extends from March 2012 to January 2020; though the first two years of data are unavailable at the Atacama Camp due to instrument error. The influence of local bias on our temperature measurements (e.g. Ishikawa, 2003; Brenning et al; 2005) is suppressed by careful site selection, i.e. on relatively flat areas covered by debris representative of the wider area, away from cliff faces, topographic depressions, and perennial snow patches (Nagy et al., 2019).

Permafrost, ground with temperatures below 0 °C for at least two consecutive years, presence can be established directly from ground temperatures (van Everdingen et al., 2005). However, where the permafrost table – i.e. the upper boundary surface of permafrost – is below the deepest temperature logger more indirect methods are necessary (e.g. Ishikawa, 2003). We build upon a detailed investigation of ground thermal regimes – i.e. ground temperature distribution, heat flows, and their time-dependence (van Everdingen et al., 2005) – on the Ojos del Salado that was carried out by Nagy et al. (2019) for the period of 2012–2016. Conclusions presented in this study provide the basis for determining the representative vertical profile of permafrost on the OSM. This aids our assessment of how permafrost and the hydrological system interacts on the OSM, e.g. how the duration and course of thawing in the active layer predetermine and modulate infiltration and recharge. Linear regression was also applied on the monthly average temperature records to determine long-term trends in ground temperature.

3.2. Ground temperature modelling

A major shortcoming of any ground temperature monitoring network is the incapability to directly obtain information about the time-dependent liquid water and ice ratio of the regolith. The presence or absence of water can be inferred by investigating temperature periodicity during freezing-thawing cycles, i.e. zero-curtain method (Outcalt et al., 1990; Nagy et al., 2019). However, with this indirect method, it is not possible to estimate the ratio of water and ice in the ground. Thus, we have developed a 1D thermal model – presented in Nagy et al. (2020) – that can be used to estimate the range of realistic water content in the ground by tuning modelled ground temperatures to observations, i.e. analysing the performance of model runs using different sets of parameters (e.g. water content).

Our model simulates temperature distribution and water/ice phase changes within the active layer to clarify interannual properties and determine any existing trends. The ground material is assumed to be a composite of liquid water, ice, rock, and air. The volumetric ratio of the fractions is time-independent, only the ratio of liquid water and ice is allowed to evolve with time. A continuous local thermal equilibrium is assumed between the ice, water, rock and air components. Hence, weighted average quantities – calculated by using the volume fractions of the different components – are used to represent the density, heat capacity and heat conduction coefficient of the composite ground material (Woodside and Messmer, 1961). The model is using a transient conduction equation with the latent heat of fusion, thus includes the effects of ice- water phase changes on the heat transfer and temperature variations (Nagy et al., 2020).

We restricted our modelling exercise to two study sites: the Atacama Camp (5260 m a.s.l.) and the Tejos Camp (5830 m a.s.l.), as these are the sites where permafrost, ice-bearing permafrost and well-developed activate layer are all present (Nagy et al., 2019). Temperature records from three data loggers (buried at 10 cm, 35 cm, and 60 cm below the surface) are used for both sites. The logger closest to the surface (i.e. at −10 cm) provides input values to the model, while the other two provides independent data streams, which are used to evaluate the performance of the model (Nagy et al., 2020).

Main assumptions of the thermal model: (1) one-dimensional geometry; (2) time independent air, water (liquid plus solid), and rock ratio; (3) constant −2.5 °C temperature at the bottom of the model domain, 5 m from the surface; the temperature was based on the observed annual mean ground temperatures at −60 cm, while the depth was based on the performance of multiple model runs with different domain depths (1–10 m, with 1 m interval); (4) the volumetric changes of water during freezing/thawing are neglected.

The key issue with this model (Nagy et al., 2020) is the difficulty of empirically determining the volume ratio of the fractions (i.e. air, rock, and water/ice) as functions of depth which is crucial for accurately simulating phase-changes and the thermal behaviour of the regolith. Nagy et al. (2019) analysed the physical properties of several regolith samples taken from multiple depths at the Atacama and Tejos Camps. As the samples exhibited weak spatial variations, an overall 60 % (v/v) porosity and rock fraction density (2700–3000 kg/m^3) was used in the model of Nagy et al., (2020). Thermal properties of the rock fraction was assumed to be similar of andesite-basalt material (Eppelbaum et al., 2014). Water content (liquid and solid) was not measured on the field by Nagy et al. (2019), thus a depth dependent but temporally fixed water content was prescribed by manually tuning modelled temperatures to the measurements (Nagy et al., 2020).

This method is labour intensive and might not arrived at the best solution due to the limited number of possible tuning experiments. Thus, we have upgraded the model to provide a more rigorous automated solution for determining the appropriate depth functions of fraction volume ratios, that provide the best match between modelled and measured temperatures. As a compromise, we describe the aforementioned depth dependence by a sparse set of parameters and employ a couple of simple assumptions: (1) the volume ratio of air is monotonically decreasing as function of depth; (2) similarly, volume ratio of rock is monotonically increasing. These simplifications enable us to automatically optimise the depth functions of fraction volume ratios by matching modelled and observed temperatures within gradient descent framework (Ruder, 2016), which is in essence the basis of deep learning (LeCun et al., 2015) and artificial intelligence schemes. Besides the parameterized depth dependent fraction volume ratios (Fig. 3), the melting point (i.e. temperature) of water is also included in the optimisation scheme as a control. This was found to be very close to 0 °C, which demonstrates that the optimisation technique did employ unphysical corrections. This also indirectly proves the presence of water.

3.3. Satellite survey of snow coverage and lake presence

As sporadic snow cover on the OSM could play a significant role in determining surface water presence and groundwater recharge, we assessed the presence of two high-elevation small lakes at 5900 m and 5890 m a.s.l. (Fig. 4) in relation to snow coverage between mid-winter of 2017 to late summer of 2020. This timeframe was chosen as we had complex field activity every summer during this period, thus we have continuous field observations to aid the interpretation of remotely sensed data.

Snow coverage and lake presence were surveyed – within the catchments of the two lakes – by using Sentinel-2 optical satellite imagery with a maximum of 10 % cloud coverage, between 2/Aug/2017 and 28/Feb/2020 (n = 88). Sentinel-2 images have been widely used to carry out high resolution surveys of surface water bodies (Kaplan & Avdan, 2017; Pena-Regueiro et al., 2020; Yang et al., 2017). Thanks to the dual satellite system, Sentinel-2 has approximately 5 days revisit frequency which makes it a useful tool for land cover mapping (Drusch et al., 2012).

Both visual inspection of true colour images (using bands 2, 3, 4) and normalised difference snow index (NDSI) products were utilised to survey snow coverage within the lake catchments. Lake presence was assessed similarly, using the same set of input satellite imagery and true colour images. However, instead of NDSI, normalised difference water index (NDWI) products (McFeeters, 1996) were calculated to aid the detection of the surface lakes. All of the aforementioned data products were created by using the Sentinel Application Platform (SNAP).

3.4. Isotope analyses of water samples

Our strategy aimed to gather samples from every key surface water types within the study area. Thus, fresh snow, and water samples were collected from the “Upper Lake” and a stream near the Tejos Camp on 25/Feb/2018. Water samples were also taken from the “Upper Lake” and “Lower Lake” on 17/Feb/2020. Besides the stream sampled near

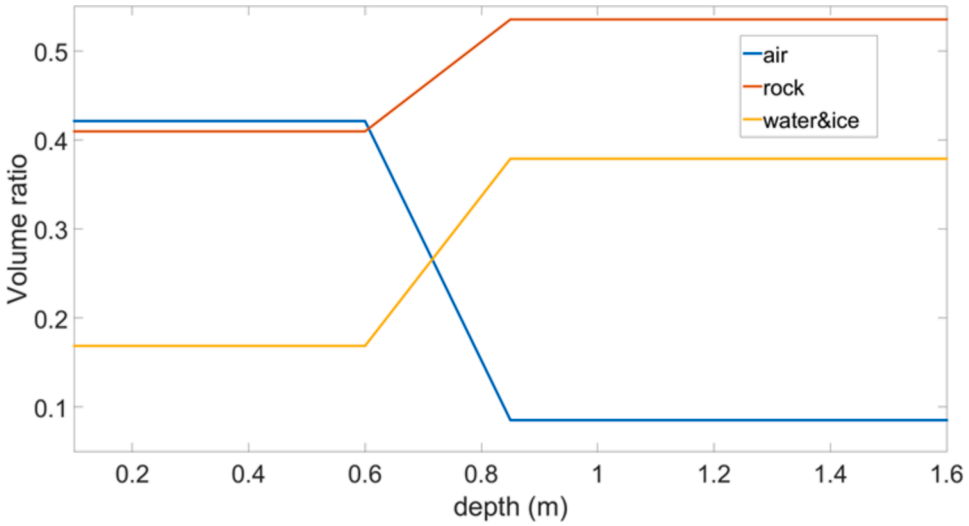

Fig. 3. Depth dependent fraction volume ratios of air, rock, and water/ice. These values are obtained using gradient descent optimisation.

Tejos Camp, a lower elevation stream near the Atacama Camp was also sampled on 19/Feb/2020 (Table 1, Fig. 4).

A depth-integrated sample was taken from the snow pack (Ala-aho et al., 2021), which represents an amount-weighted average of the snow events during the weeks preceding the sampling date. Following the principles of Clark & Fritz (1997), the samples were then packed into air-tight plastic bags and poured into bottles once molten. Since the melting process took place in hermetically sealed plastic bags, isotopic changes are prevented (Dietermann & Weiler 2013). From surface waters, grab samples were collected in 500 mL HDPE containers leaving only minimal headspace and were closed tightly to avoid leakage or evaporation. Isotope analyses were carried out on the water samples to estimate the potential contribution of different water sources such as present-day precipitation, 'old' or 'young' water from the thawing permafrost (Gibson et al., 2016, Wan et al., 2019), or potential geothermal sources which are frequently described across the volcanic Andean Cordillera, including northern Chile (Houston 2007, Tassi et al., 2010). A peculiar geothermal fluid generally associated with andesitic magmatism is recycled seawater, called "andesitic water" (Giggenbach, 1992). If such component discharges to the studied surface waters it might complicate the isotopic interpretation.

In the lab, a few mL water was sub-sampled from each container for stable isotope analyses. The rest of each sample was distilled and filled into metal canisters. After degassing, the metal canisters were closed and stored for several months to allow ^{3}He ingrowth from tritium decay. Finally, the canisters were connected to the inlet line of a noble gas mass spectrometer (Helix SFT) and the He fraction was allowed to enter the dual collector mass spectrometer. ^{3}He and ^{4}He were measured simultaneously, applying the peak height method. During the sample intake, an ultrapure ^{4}He spike was added to each sample (Palcsu et al., 2010). Tritium activity is expressed in tritium units (1 TU equals to the ^{3}H/H ratio of 10^{-18}, and corresponds to an activity concentration of 0.119 Bq/L). The overall precision of the tritium measurements is usually better than 2.0 % above 1 TU, if sample size is larger than 500 mL.

Measured tritium activities are compared to decay corrected reconstructed tritium activities of precipitation to help determine the origin of contemporary surface water on the OSM. Reconstructed annual mean regional precipitation ^{3}H activities have been retrieved from a set of regional records for the temperate zone of South America (Basaldúa et al., 2022). The region situated closest to the OSM was selected from this dataset. The importance of using the closest reference for tritium background level from precipitation to the examined area is underlined by Tazioli et al. (2022). These reconstructions, available from 1960 to 2022 (Basaldúa et al., 2022), were corrected for radioactive decay using the estimated ^{3}H half-life of 12.32 years (Lucas and Unterweger, 2000) before comparisons with the measured tritium activities of our samples.

The stable hydrogen and oxygen isotope composition of the samples was determined by laser spectroscopy. Samples collected in 2018 were analysed by a Liquid Water Isotope Analyzer (LWIA-24d, Los Gatos Research) at the Institute for Geological and Geochemical Research, Budapest, Hungary. Samples and laboratory standards were pipetted into 2 mL vials, 1 μL specimens from these vials were injected into the vaporizer of the laser analyser where they were evaporated at 80 °C in low vacuum. Although 6 injections were made from each vial, only the latest four measurements were used to determine the isotope composition of the samples to minimize memory effect (Czuppon et al., 2021). All samples were measured at least two times. The laboratory standards, calibrated to international standards BWS1, BWS2 and BWS, have the following composition: δ^{2}H = –9.0 ‰; –74.9 ‰; –147.7 ‰; and δ^{18}O = –0.53 ‰; –10.41 ‰; –19.95 ‰, respectively. Samples collected in 2020 were analysed by a Liquid Water Isotope Analyzer (LGR LWIA-24i, ABB-Los Gatos Research) at the Institute for Nuclear Research, Debrecen, Hungary. Stable hydrogen and oxygen isotope composition of the water samples are expressed as δ^{2}H and δ^{18}O in ‰ relative to V-SMOW (Vienna Standard Mean Ocean Water) (Coplen 1994). The reproducibility considering both datasets is better than 1.0 ‰ and 0.15 ‰ for δ^{2}H and δ^{18}O, respectively.

3.5. Developing a conceptual hydrological model

Previous hydrological datasets and analyses were combined with new information obtained in this study and theoretical considerations to develop a conceptual model that characterises the current hydrological configuration – i.e. water sources and their connectivity – of the OSM headwaters. We utilised a simplified hydrological budget equation, developed for permafrost affected glacial forelands (Cooper et al., 2011), as a guide for the conceptual framework:

$$W_F = W_P + W_R - W_E - W_{SSS} - W_{SR} \pm W_{\Delta W_s} \quad (2)$$

where the main channel net water flux (W_F) consists of; precipitation (W_P), channel recharge from the active layer (W_R), evaporation (W_E), sub-surface seepage (active layer discharge outside channel) (W_{SSS}), surface runoff (W_{SR}) and the change in the water storage ($W_{\Delta W_s}$).

Information about surface hydrology in the region was obtained from previous field reports of the local Water Directory: D.G.A. Chile (DGA-Arcadis, 2015; Vargas Paysen, 2013; Enguita, 2016) and the PermaChile network (Földgömb Foundation, Hungary). Ground thermal regime datasets from field studies (Nagy et al., 2020) were also used to

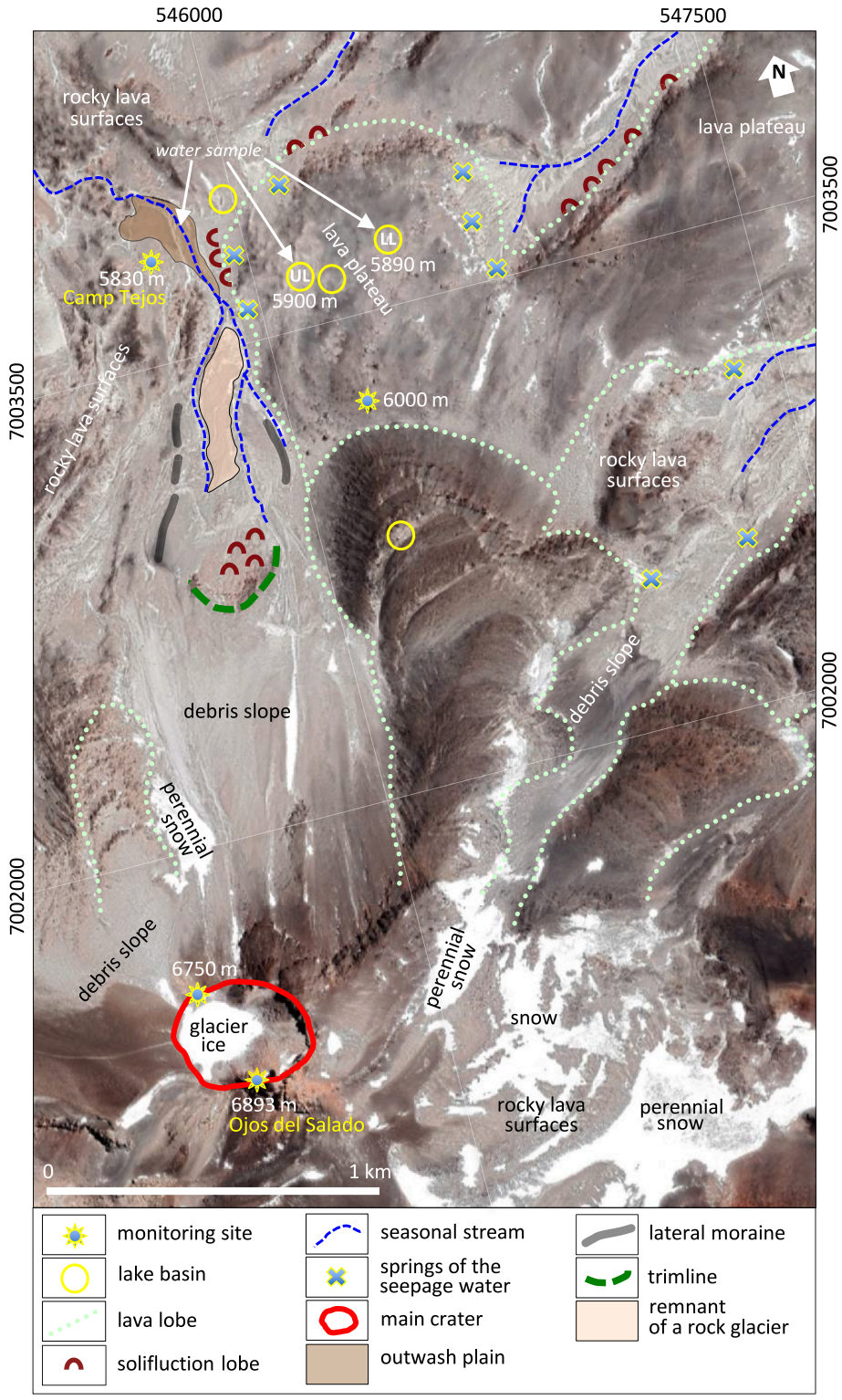

Fig. 4. An inset satellite image showing lavalobes, lake basins, and surface streams on the northern slope of the Ojos del Salado summit; UL: Upper Lake, LL: Lower Lake.

evaluate surface conditions that could modify infiltration and subsurface hydrological dynamics at preferential recharge sites. Our conceptual hydrological model can be used to evaluate current hydrological organisation and the possible future pathways of its evolution.

4. Results

4.1. Timing and length of ground thawing

The ground temperature model – using continuous, long-term hourly temperature measurements and automated gradient descent optimisation of air-rock-water volume ratios (Section 3.2) – allowed us to

Table 1
Date and location of sampling around the OSM in 2018 and 2020 collected for isotope hydrological analysis.

Code	Site	Date	Lat	Lon	Alt (m a.s.l.)
OS-2018-1	Snow	25/Feb/2018	27°05′19.20″ S	68°32′04.50″ W	5910
OS-2018-2	"Upper Lake"	25/Feb/2018	27°05′18.70″ S	68°32′03.40″ W	5900
OS-2018-3	Stream (Tejos)	25/Feb/2018	27°05′16.90″ S	68°32′13.50″ W	5825
OS-2020-1	"Upper Lake"	17/Feb/2020	27°05′18.70″ S	68°32′03.40″ W	5900
OS-2020-2	"Lower Lake"	17/Feb/2020	27°05′18.40″ S	68°31′51.53″ W	5890
OS-2020-3	Stream (Tejos)	19/Feb/2020	27°05′16.90″ S	68°32′13.50″ W	5825
OS-2020-4	Stream (Atacama)	19/Feb/2020	27°03′31.20″ S	68°32′58.48″ W	5240

investigate the vertical profile of thawing/freezing in the active layer and the associated phase changes of water. As we have no measurements from depths larger than −60 cm which could be used to constrain our model, we focus on the interpretation of model outputs for the uppermost 60 cm of the ground. This almost completely covers the actual thickness of the active layer at the Tejos Camp, while at the Atacama Camp the coverage is partial (Nagy et al., 2019) (Fig. 5).

Results of the temperature modeling are presented graphically (Fig. 5). Accuracy of the model was assessed by comparing the presence of daily ground temperature periodicity – which is a key indicator of thermal and phase-change processes in the active layer (Nagy et al., 2019; 2020) – in the observed and modeled temperature signals (Text S1, Table S1). Observed and modelled daily mean temperatures are also compared directly to aid this evaluation (Text S1, Table S2). Both tests – and the visual comparisons – suggest that our model performs well and captures the thermal evolution of the ground with sufficient accuracy.

Our modelling for the Tejos Camp indicated that positive ground temperatures and phase changes are common at shallow depths, though the active layer is typically thinner than 1 m (Fig. 5). The thickness of the active layer exhibits a notable (>20 %) interannual oscillation, reaching

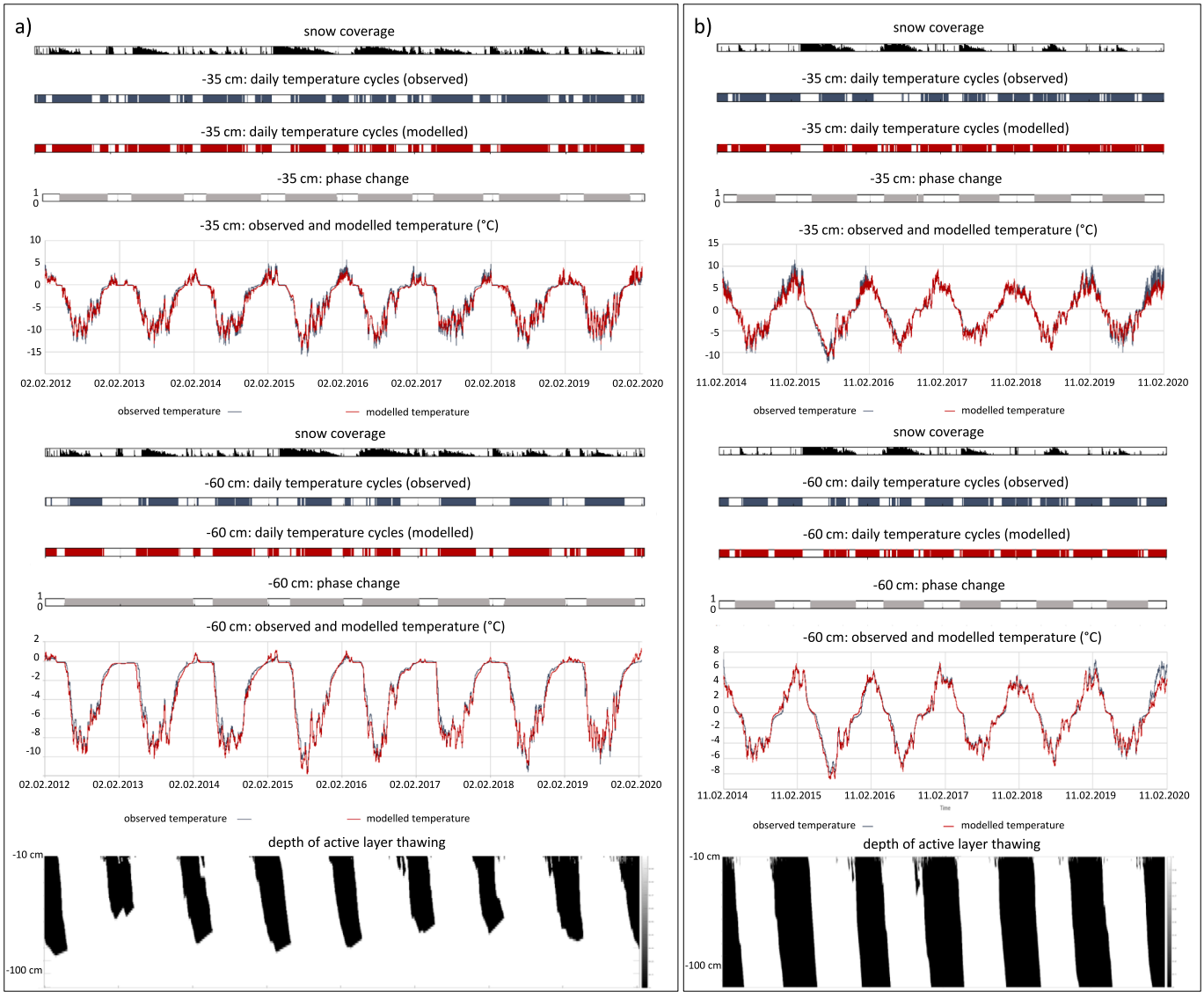

Fig. 5. (a) Measured and modelled temperature at the Tejos Camp, 5830 m a.s.l., (b) and at the Atacama Camp, 5260 m a.s.l. Phase change in the ground is graded from 0 (completely liquid) to 1 (completely solid).

only about 55–60 cm in La Niña years (e.g. 2012/13, 2016/17, 2017/18), and > 70 cm in El Niño years (Fig. 5). Although, confidence levels are lower in the latter case as the active layer extends deeper than our model constraints, the scale of this extrapolation is small (< 20 cm). Hence, we propose that the ground thermal model can provide a full picture about the evolution of the active layer at the Tejos Camp.

Ground thaw at 35 cm depth usually starts in the second half of December, or the beginning of January, while at 60 cm depth it starts about 23–39 days later (Fig. 5, Table S3). Thawed ground usually persists for about 105–120 days per year (about 24 % of the investigated period) at 35 cm depth, although this can be considerably shorter in some years, e.g. in 2017/18 it lasted for only 80 days. Ground stays thawed for shorter periods with increasing depth, e.g. at 60 cm it lasts for about 90–112 days per year (Fig. 5, Table S3).

The active layer is thicker and ground thawing lasts longer at the Atacama Camp. According to the model results, the ground is thawed at 35 cm depth for about 45.8 % of the investigated period. At 35 cm depth, thawing usually starts in November, though this varies significantly between different years (Fig. 5, Table S3). The start of thawing only lags about 5–12 days behind at the depth of 60 cm. The ground stays thawed for about 160–180 days at 35 cm depth. At 60 cm depth, this period is only about 5–8 days shorter, though in many summer seasons there is virtually no difference (Fig. 5, Table S3). Hence, thawing propagates towards larger depths quickly, while the length of the thawed period does not vary significantly close to the surface at the Atacama Camp, in contrast to the Tejos Camp. The complete refreezing of the ground is usually achieved by April and May at both sites (Fig. 5, Table S3). As the modelled thickness of the active layer extends well beyond the model constrains during each summer (Fig. 5), we cannot estimate the actual thickness of the active layer at the Atacama Camp with sufficient confidence.

4.2. Presence of surface snow and water

High-altitude lakes on the OSM are formed in depressions on the flat tongues of former lava flows, in basins between lavalobes, within tributary craters, and behind parasitic cones. We investigated two regularly recurring lakes on the OSM – the "Upper Lake" (UL) and "Lower Lake" (LL) – in the 5890–5900 m zone (Fig. 6). The area around the two larger lakes (UL and LL) has been field surveyed five times between 2014 and 2020. Apart from 14/Jan/2019 the presence of these lakes were confirmed on the field (Fig. 6h). Although field surveys are useful for ground validation, they only provide a short snapshot about the temporal evolution of the lakes; e.g. in 2019 satellite images indicate that the lakes appeared in February, similarly to other years, a few weeks after our field visit (Fig. 6). Satellite image surveys between Aug/2017 and Feb/2020 reveal that open water in the lake basins usually appears in the second half of the summer – i.e. from February onwards (Fig. 6). This is several months later than the start of ground thawing within the 5800–6000 m a.s.l. elevational zone, starting in November (Fig. 5). Open water within the lake basins was usually present for about 6–8 weeks during each summer, after this time the water either drained away and/or a thin ice layer formed in the shallow ponds for the first half of the winter.

The timing of lake appearance in this elevational zone suggests an inverse connection with the seasonal evolution of active layer thickness. Early in the melt season, until January, the active layer is very thin, below 20 cm (Fig. 5). Although the water storage and seepage capacity of this thin active layer is small, meltwater infiltrates and seeps away instead of accumulating in meltwater ponds. Lakes only appear within poorly drained areas around mid-summer, when the active layer reaches the thickness of ~ 50 cm and its growth rate slows down (Figs. 5, 6). Later during the summer, as water saturation in the active layer becomes more widespread, groundwater seepage overflows the lava plateaus and small, short-lived springs form on the slopes of lava lobes (Fig. 4). In

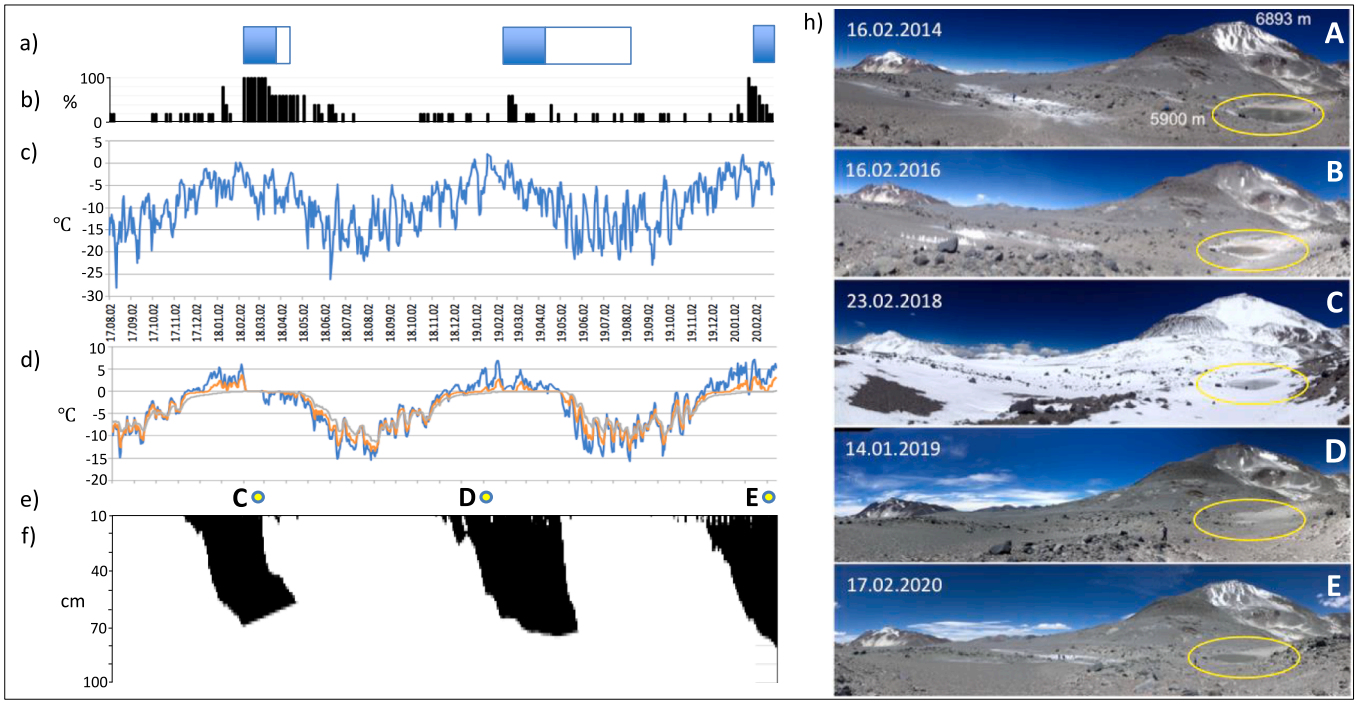

Fig. 6. (a) Generalised presence of the two regularly occurring lakes (UL, LL) in the 5890–5900 m zone (blue: open water, white: lake-ice) between 02/Aug/2017 and 28/Feb/2020. (b) Snow coverage within the catchment area of the lakes. (c) Daily mean air temperatures (2 m above the surface) measured at 6000 m a.s.l. near the lake sites. (d) Daily mean ground temperatures (blue: −10 cm; orange: −35 cm; grey: −60 cm) measured at the nearby Tejos Camp at 5830 m a.s.l. (e) Dates when field observations and photos are available for the UL; see panel (h). (f) The binary mask indicates the modelled evolution of the active layer at the nearby Tejos Camp (Fig. 3). (h) Photographs showing the site of the Upper Lake (UL) on different dates. (For interpretation of the references to colour in this figure legend, the reader is referred to the web version of this article.)

parallel with this, small surface streams also appear as the melt season progresses. These streams are fed either by the aforementioned springs (5800–6000 m a.s.l.) or by melting perennial snow patches (Fig. 4), especially at higher elevations (6200–6300 m a.s.l.). Observations from 2018/19 indicate, that the presence of significant snow coverage is not a strong prerequisite of lake formation. Even though only light snow coverage was detected in the preceding winter, lakes do appear as usual in February (Fig. 6). However, major snowfall events in the summer strongly promote the formation and growth of lakes and meltwater ponds due to the quick saturation of the active layer by the melting snowpack.

4.3. Isotope compositions of the surface waters

Stable hydrogen and oxygen isotope composition of fresh snow samples collected in late February 2018 were −69.5 ‰ for δ^2H and −10.33 ‰ for $\delta^{18}O$, the ^3H activity was 5.36 ± 0.10 TU. Stable isotope composition of surface waters collected around the OSM in 2018 and 2020 ranged from −114.3 to −31.4 ‰ for δ^2H, and from −15.32 to −2.0 ‰ for $\delta^{18}O$ (Table 2). Tritium activities of the samples ranged from 4.7 to 8.7 TU (Table 2). ^3H activities of fresh snow samples collected by us in 2018 (Table 2) and by an independent study in 1990 (6.22 ± 0.38 TU, Grosjean at al., 1995) agree within uncertainty with the corresponding reconstructed annual mean precipitation ^3H activity of Basaldúa et al. (2022), which were obtained for a nearby region. This supports using this reconstruction as reference for the evaluation of the ^3H activities of surface waters and groundwater from the OSM region.

5. Discussion

5.1. Contemporary configuration of surface hydrology

Snow coverage on the OSM above 5000 m a.s.l. exhibits strong annual and seasonal variations, while rain is rare. Thus, snow presence and melting determines the supply of liquid water. Permafrost occurrence becomes widespread above ~ 5200 m a.s.l. on the OSM; this also needs to be considered in the hydrological budget as infiltration and recharge is confined by the permafrost table, while storage and seepage can also occur at shallow depths in the active layer (Fig. 7). The evolution of the snowpack also impacts the timing and length of ground thawing due to its insulating effect (Fig. 5) (Nagy et al., 2019). This in turn affects the thickness of the active layer and its capacity for infiltration and groundwater seepage, and has consequences for the depth and horizontal coverage of the permafrost table. Hence, at high elevations on the OSM infiltration is restricted to preferential recharge zones that are controlled by the downslope convergent topography (Carroll et al., 2019), and the spatiotemporal distribution of permafrost (Fig. 7),

Table 2
Tritium activity and stable isotope composition of snow and surface waters collected around the OSM in 2018 and 2020.

Sample code	Sampling site	^3H(TU)	δ^2H_{VSMOW} (‰)	$\delta^{18}O_{VSMOW}$ (‰)
OS-2018-1	snow	5.36 ± 0.10	−69.5	−10.33
OS-2018-2	"Upper Lake"	5.54 ± 0.11	−72.2	−10.15
OS-2018-3	stream (Tejos)	5.61 ± 0.11	−90.2	−12.70
OS-2020-1	"Upper Lake"	8.71 ± 0.33	−31.4	−2.01
OS-2020-2	"Lower Lake"	6.93 ± 0.36	−36.9	−4.14
OS-2020-3	stream (Tejos)	6.11 ± 0.36	−60.5	−7.22
OS-2020-4	stream (Atacama)	4.72 ± 0.36	−114.3	−15.23

active layer, and snow coverage. This further complicates the already significantly restricted recharge due to the strong evaporation and sublimation in this arid environment; i.e. recharge is only about 5–10 % of the precipitation in lower altitude arid areas near the OSM, e.g. the alluvial basins at 27°S (Enguita, 2016).

Based on our ground temperature measurements and thermal model, freeze–thaw cycles occur in the ground at both the Tejos and Atacama Camps. Strong early and late summer thawing-freezing cycles without significant zero curtain periods are typical at shallow depths of the Atacama Camp. However, similar cycles also occur at the Tejos Camp, especially in the early summer (e.g.: Dec/2012, Dec/2016, Dec/2018). Snow coverage affects these cycles at both locations. These transitional periods are characterised by large and abrupt changes in the conductivity and storage capacity of the active layer. As the melt season progresses, and snow coverage becomes insignificant, the ground remains thawed at shallow depths. Thawed ground (i.e. active layer with liquid water) is present for about 32 % and 39 % of the observation period at the Tejos and Atacama sites respectively. Hence, the active layer can be considered a seasonal shallow unconfined aquifer (Fig. 7), which gets thicker during the melting season – reaching about 60 cm – and thus provides a deepening confinement table for infiltration. Infiltration and shallow groundwater seepage can also be disrupted by short-term (lasting 1–2 weeks) refreezing events, e.g. during late summer at the Tejos site, before ceasing completely at the end of summer. The change in subsurface water storage ($W_{\Delta Ws}$) at the end of the melt season, when main channel water flow is paused due to freezing (i.e. $W_F = 0$), equals with the recharge (W_R) minus the active layer discharge (W_{SSS}), according to the site specific hydrological budget (Eq. (2). The active layer is thicker/deeper and it is present for a longer time (+7% of the observed period) at the Atacama Camp than at the Tejos Camp. Thus, considering similar magnitudes and timing of precipitation, evaporation, and recharge – which is a reasonable assumption given the close proximity of the two sites – change in active layer storage at the end of the melt season is expected to be significantly more negative at the Atacama Camp than at the Tejos Camp due to larger active layer discharge.

Although meltwater form the snowpack (Table 3) – and perennial firn patches in sheltered locations – can infiltrate to the active layer and towards larger depths through permafrost discontinuities and rock fractures, this is strongly inhibited where the active layer is shallow and permafrost is widespread/continuous, especially above ~ 5600 m a.s.l. (Nagy et al., 2019; 2020). Hence, a highly transient surface hydrological network consisting of meltwater ponds and streams can form within the wider permafrost zone – i.e. continuous and discontinuous permafrost between ~ 5000–6500 m a.s.l. (Nagy et al., 2019; 2020) – during the summer Table 3. Shallow seasonal meltwater ponds also form in this zone, i.e. within the elevational range of ~ 5800–6300 m a.s.l. These ponds can appear even in the absence of significant snow coverage, thus active layer discharge (W_{SSS} in Eq. (2) likely plays an important role in their formation. This water could be sourced from melting ground ice and stored surface meltwater (i.e. from the melting snowpack and firn patches). Landforms generated by thermal erosion and thaw slumping (Nagy et al., 2020; Kereszturi et al. 2022) – e.g. near the Atacama Camp at 5200 m a.s.l. – and transient meltwater ponds (Aszalós et al., 2020) corroborate the presence and degradation of ground ice, suggested by the analysis of ground temperature records (Nagy et al., 2019). These features could also indicate preferential recharge sites due to the presence of a highly porous mixture of regolith and ground ice (Nagy et al., 2020), and a disturbed permafrost table. Liquid surface water is unlikely to appear at higher elevations – above ~ 6500 m a.s.l. – as temperatures only rise above 0 °C occasionally (Nagy et al., 2019, 2020) and sublimation is strong.

5.2. Surface and near-surface hydrological connectivity

Hydrological connectivity can be inferred from the isotopic signatures of our samples. Stable isotope compositions of the surface water

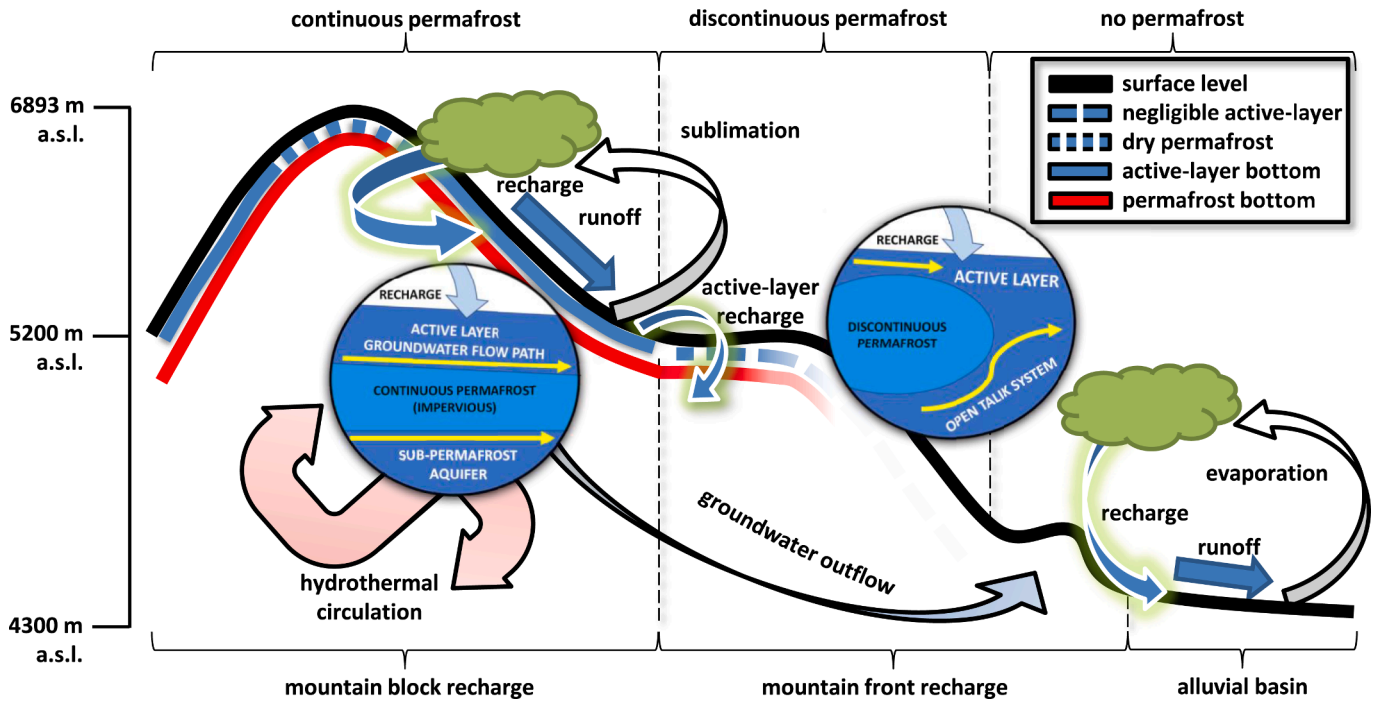

Fig. 7. The conceptual model of surface hydrology on the OSM.

Table 3
Summary of main hydrological structures of the Ojos del Salado massif.

Feature	Altitudem a.s.l.	Attribute	Reference
Transient seasonal high-altitude lakes	5200–6500	Small and shallow with about 0.8–1.4 m depth	Aszalós et al., 2016; Nagy et al., 2020
Seepage slopes	5830–6000	Lavalobes connecting plateaus with shallow lakes	Nagy et al., 2020
Thaw slumping (thermokarst)	5200	Slumps are 1–3 m in diameter	Nagy et al., 2020; Kereszturi et al. 2022
Retrogressive thaw slumps	5200	Due to melting of firn buried within steep sand headwalls	Nagy et al., 2020
Surface streams	4900–6300	Currently ephemeral with strong diurnal and seasonal variations; relict fluvial valleys	This study
Perennial snow patches	>5900	Associated with preferential recharge areas	Nagy et al., 2020

samples from the OSM are within the range of compositions measured for precipitation samples in northern Chile (Jordan et al., 2019; Boschetti et al., 2019). Snow and stream water samples exhibit a relatively more depleted composition and fit well to the Northern Chile meteoric waterline (Boschetti et al., 2019), while lake water samples usually show relatively more enriched composition and are scattered below it (Fig. 8a), indicating some evaporation effect (Craig et al., 1963). The regression line fitted to lake water data does not point to the field of „andesitic water" (Fig. 8a), which indicates that this is not a component in the mixing process (e.g. Tassi et al., 2010). The source composition of lake water is estimated by a back extrapolation to the meteoric waterline along the empirical evaporation line (Gat 1995). According to this, the estimated source composition of lake water is consistent with the stable isotope composition of snow and stream waters (Fig. 8a). These results suggest that 1) high altitude summer lakes on the OSM are recharged by snowmelt and streams, and 2) lake water is isotopically modified at the air–water interface due to evaporation, as expected in such a dry environment (Gat 1995). In conclusion, the stable isotope composition of all our samples from streams and lakes within the permafrost belt of the OSM suggest meteoric origin.

For the period between 2018 and 2020, tritium (^{3}H) activities from ephemeral streams and lakes align with measurements taken from the fresh snow samples (Table 3, Fig. 8b) – collected near the Upper lake in 2018. The tritium signal also broadly aligns with independent measurements made at another high elevation site in the North Chilean Andes (Kinnard et al., 2020) and the Andean background level (Houston 2007). Considering reconstructions of the annual mean tritium activity in precipitation for the OSM region (Basaldúa et al., 2022), the decay-corrected activity is steadily below 4 TU before 2012 (Fig. 8b). The tritium activity of our samples collected from surface waters was above 4 TU without exception. Thus, we propose that if water from the thawing permafrost is a major source of surface water (i.e., lakes and streams), then this water in the period of 2018–2020 could not have been replenished before 2012. This means that the main fraction of the active layer and surface water is young, with multiannual storage under 8 years pertaining to 'perennial' snow cover and snowmelt sources as well. Recent reports about snowpack burial (Nagy et al., 2020) and thawing in subsequent melt seasons (Kereszturi et al., 2022) support this interpretation.

We must emphasize that the small sample set is a key limitation complicating the interpretation of the data. A more robust dataset using additional samples, representing a larger temporal and spatial coverage, could help to characterise the hydrological processes influencing isotopic signatures more precisely. We propose that it would be especially important to discern whether the observed variability is primarily due to internal hydrological processes – such as evaporation – or external factors, like differences in the isotopic composition of precipitation between sampling years.

5.3. *Future evolution of surface hydrology and sources of uncertainty*

The spatiotemporal distribution of permafrost and the state of the active layer (thickness, water content, seasonal evolution, etc.) are

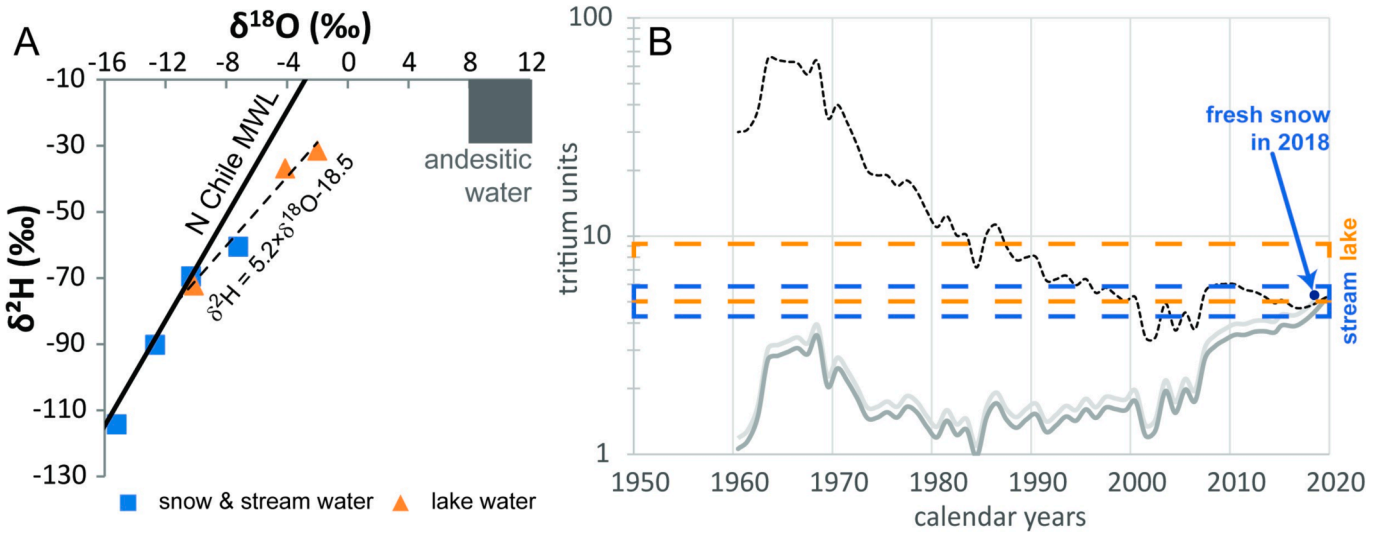

Fig. 8. Isotope hydrological characteristics of surface waters of the OSM. a) Stable hydrogen and oxygen isotopes and b) ^{3}H activities of the samples collected from fresh snow and the range for stream waters (blue) and lake waters (orange) in 2018 and 2020. The Northern Chile Meteoric Waterline (N Chile MWL, Boschetti et al., 2019) and the empirical evaporation line fitted to the lake water data are shown with solid and dashed lines, respectively. The "andesitic water" field (Giggenbach, 1992) is marked by the grey rectangle in panel A. The regional estimates of mean annual ^{3}H in precipitation (Basaldúa et al., 2022) is shown as a thin black curve. The decay corrected activities calculated for 2018 (light gray) and 2020 (dark grey) must be considered as references when assessing ^{3}H activities of our samples. (For interpretation of the references to colour in this figure legend, the reader is referred to the web version of this article.)

among the main controls of the hydrological system in periglacial regions (Bockheim, 2015; Wang et al., 2009). The extension of the sporadic (i.e. low probability) permafrost zone on the OSM under future RCP atmospheric warming scenarios could lead to widespread permafrost degradation (Ruiz Pereira et al., 2021), modifying recharge and infiltration patterns in the permafrost zone (Hiyama et al., 2013; Markovich et al., 2019; Sjöberg et al., 2021). Therefore, evaluations of the changing hydrological regime of cold-dry environments (Arenson et al., 2022), such as the OSM, should consider changes in active layer storage (Evans & Ge, 2017) and groundwater recharge (Kuchment et al., 2000) due to permafrost degradation. Nevertheless, the sensitivity of shallow interstitial ice to changes in moisture and temperature forcing is uncertain at high altitudes (>5000 m a.s.l.) on the OSM, and similar cold deserts. These uncertainties are propagated when assessing the responses of groundwater flow, and the response time, to surface climatic changes in cold deserts (Cuthbert et al., 2019) especially beyond the next century (Bense et al., 2009).

Finally, surface, and subsurface hydrological processes and their interplay on the OSM are likely to be influenced by hydrothermal circulation. For example, hydrothermal influx under the lower boundary of permafrost (Fig. 7) could imply a secondary recharge from stored subsurface relict ice. This interaction is largely unknown on the OSM, with inherent uncertainty stemming from the unknown thickness of the permafrost layer. This is heavily controlled by the geothermal gradient and ranges broadly even on active volcanoes; i.e. from hundreds of metres where the gradient is low (Abramov et al., 2008; Goyanes et al., 2014) to just a few metres where the gradient is high, e.g.: Chajnantor Volcano (22°59′S, 67°44′W) where a 200 °C/km geothermal gradient limits permafrost table to 5 m depth at 5000 m a.s.l. (Mena et al., 2021).

As no evidence of hydrothermal activity (e.g. thermal springs, fumaroles) were found near our study sites, we believe that our interpretation of the surface and near-surface (i.e. active layer) hydrological system is valid and that hydrothermal circulation mostly affects processes at larger depth. However, it is not possible to comprehensively assess the hydrogeological situation of the Ojos del Salado – and place it within a basin-scale hydrogeological framework – until more information is available, e.g. permafrost thickness, large-scale hydrogeological connectivity. Thus, more research is needed that is capable of exploring processes at larger depths, e.g. ground-penetrating radar and borehole measurements. This would provide additional field validation to our current findings about the surface and near-surface hydrology of the OSM, e.g. by further constraining the spatiotemporal distribution of permafrost. More importantly, resolving the hydrogeological context of the OSM – by connecting surface and near-surface processes with basin-scale flow patterns – will aid propagating the downstream effects of climatic impacts and pollution (e.g. from mining or tourism) on the OSM and similar high altitude massifs in the region. Thus, such research is crucial for the water security of the Atacama region, and potentially to other similar environments.

6. Conclusions

A transient surface water network – consisting of ephemeral lakes and streams – is present between ~ 4900 and 6500 m a.s.l. on the OSM. Seasonal lakes – depressions and behind dams of volcanic debris – are most abundant in the elevation range of 5800 to 6100 m a.s.l. which is also associated with the high probability presence of both permafrost and ground ice, which constitute a subsurface layer with low permeability. Surface water originates from local snowmelt and active layer discharge – supplied by infiltration and seepage and/or in-situ thawing of ground ice. During most of the year lake basins are dry or hosting small patches of snow and ice. However, these basins fill up with meltwater (0.5–2 m deep) during the first half of the summer, and the resulting lakes persist for about 6 to 8 weeks, through late summer and the autumn transition period.

Seasonal surface streams can occur in the elevation range between 4900 and 6500 m a.s.l., though they are the most abundant above 5500 m a.s.l. where permafrost hinders deep infiltration and seepage and there are plenty of water sources. Like lakes, streams are fed by melting seasonal and perennial surface snow patches and also by active layer discharge. The latter is especially important in the zone of 5800 to 6100 m a.s.l., where lakes are also the most abundant. Here, the active layer is relatively thick so it can store a significant amount of water, the permafrost table is mostly continuous so it hinders deep infiltration and seepage, and there are ample water sources so the active layer can become saturated during the melt season. Streams usually have a shorter life span than lakes, lasting around 2 to 4 weeks during the summer. Stable isotope compositions and tritium activities both suggest that the

water in ephemeral streams and lakes originates from recent (< 10 years old) precipitation. However, further investigation with a larger dataset and consideration of external meteorological factors would be necessary to fully understand the processes affecting the isotopic composition in these areas.

Above 6500 m a.s.l. the formation of a surface hydrological network is strongly inhibited by the cold temperatures, which limit thawing to a few hours during the summer and make the active layer virtually absent. Here, sublimation is the dominant process that reduces the thickness of the snowpack and causes the drying out of the top layers of the regolith. Thus, even if temperatures allow some melting, this meltwater will quickly infiltrate and refreeze in the ground. The formation of a surface hydrological network is also inhibited below 4900 m a.s.l. due to the low probability of permafrost (i.e. sporadic permafrost), which do pose any considerable hindrance to infiltration. Water sources are also scarce in this zone due to lower precipitation and the scarcity of ground ice. Thus, meltwater produced locally or transported via surface streams infiltrates quickly towards deeper layers, possibly contributing to groundwater recharge, though the volumes of this water is likely low. Hence, we suggest that the thermal regime of the ground – which determines the distribution and seasonal evolution of the permafrost and the active layer – plays a preponderant role in the characteristics and evolution of surface hydrology and recharge on the OSM and similar high altitude massifs in the Dry Andes.

The permafrost zone is expected to drift towards higher elevations and the active layer is expected to become thicker at a given altitude in the future, due to the predicted warming. Thus infiltration towards deeper layers will become less restricted, and the storage capacity of the active layer will increase. Unless significant surplus meltwater becomes available from the region above 6000 m a.s.l. – e.g. from ground ice or buried and surface snow patches – this process will fundamentally reduce the seasonal presence of surface water. Thus, future climatic changes could significantly change recharge patterns through their effect on permafrost. We suggest that this interplay should be considered when evaluating future hydrological pathways and water security in the region. However, more research is needed, especially about conditions and processes at larger depths that influence regional flow patterns, and about meteorological parameters (e.g. precipitation, evaporation, sublimation) which determine the surface water budget.

CRediT authorship contribution statement

Balázs Nagy: Writing – original draft, Resources, Project administration, Methodology, Investigation, Funding acquisition, Formal analysis, Conceptualization. **Sebastián Ruiz-Pereira:** Writing – original draft, Visualization, Methodology, Investigation, Conceptualization. **Ádám Ignéczi:** Writing – review & editing, Writing – original draft, Investigation, Conceptualization. **József Kovács:** Methodology, Investigation, Formal analysis, Data curation, Conceptualization. **Kaveh Ghahraman:** Investigation, Conceptualization. **Gábor Mihajlik:** Writing – original draft, Software, Methodology, Formal analysis. **Marianna Túri:** Methodology, Formal analysis. **Zoltán Kern:** Writing – review & editing, Writing – original draft, Methodology, Investigation, Formal analysis, Conceptualization.

Declaration of competing interest

The authors declare that they have no known competing financial interests or personal relationships that could have appeared to influence the work reported in this paper.

Appendix A. Supplementary data

Supplementary data to this article can be found online at https://doi.org/10.1016/j.jhydrol.2025.132741.

Data availability

Data will be made available on request.

References

Abramov, A., Gruber, S., Gilichinsky, D., 2008. Mountain permafrost on active volcanoes: field data and statistical mapping, Klyuchevskaya volc DGA-Arcadis, 2015ano group, Kamchatka. Russia. Permafrost and Periglacial Processes 19 (3), 261–277.

Ala-aho, P., Welker, J.M., Bailey, H., Højlund Pedersen, S., Kopec, B., Klein, E., Mellat, M., Mustonen, K.-R., Noor, K., Marttila, H., 2021. Arctic snow isotope hydrology: a comparative snow-water vapor study. Atmos. 12 (2), 150.

Alvarez-Garreton, C., Boisier, J.B., Garreaud, R., Seibert, J., Vis, M., 2021. Progressive water deficits during multiyear droughts in basins with long hydrological memory in Chile. Hydrol. Earth Syst. Sci. 25, 429–446.

Arenson, L.U., Harrington, J.S., Koenig, C.E., Wainstein, P.A., 2022. Mountain permafrost hydrology—a practical review following studies from the Andes. Geosciences 12 (2), 48.

Aszalós, J.M., Krett, G., Anda, D., Márialigeti, K., Nagy, B., Borsodi, A.K., 2016. Diversity of extremophilic bacteria in the sediment of high-altitude lakes located in the mountain desert of Ojos del Salado volcano. Dry-Andes. Extremophiles 20 (5), 603–620.

Aszalós, J.M., Szabó, A, Felföldi, T, Jurecska, L, Nagy, B, Borsodi, AK., 2020 Jun. Effects of Active Volcanism on Bacterial Communities in the Highest-Altitude Crater Lake of Ojos del Salado (Dry Andes, Altiplano-Atacama Region). Astrobiology 20 (6), 741–753. https://doi.org/10.1089/ast.2018.2011.

Baraer, M., Mark, B.G., McKenzie, J.M., Condom, T., Bury, J., Huh, K.-I., Portocarrero, C., Gómez, J., Rathay, S., 2012. Glacier recession and water resources in Peru's Cordillera Blanca. J. Glaciol. 58 (207), 134–150.

Barnett, T.P., Adam, J.C., Lettenmaier, D.P., 2005. Potential impacts of a warming climate on water availability in snow-dominated regions. Nature 438 (7066), 303–309.

Basaldúa, A., Alcaraz, E., Quiroz-Londoño, M., Dapeña, C., Ibarra, E., Vélez-Agudelo, C., Copia, L., Martínez, D., 2022. Reconstruction of the record of tritium in precipitation in the temperate zone of South America. Hydrol. Process. 36 (9). https://doi.org/10.1002/hyp.14691.

Bense, V.F., Ferguson, G., Kooi, H., 2009. Evolution of shallow groundwater flow systems in areas of degrading permafrost. Geophys. Res. Lett. 36 (22). https://doi.org/10.1029/2009GL039225.

Bockheim, J.G., 2015. Global distribution of cryosols with mountain permafrost: an overview. Permafr. Periglac. Process. 26 (1), 1–12.

Boisier, J.P., Alvarez-Garretón, C., Cordero, R.R., Damiani, A., Gallardo, L., Garreaud, R. D., Lambert, F., Ramallo, C., Rojas, M., Rondanelli, R., 2018. Anthropogenic drying in central-southern Chile evidenced by long-term observations and climate model simulations. Elementa Sci Anth 6 (1), 74. https://doi.org/10.1525/elementa.328.

Boschetti, T., Cifuentes, J., Iacumin, P., Selmo, E., 2019. Local meteoric water line of Northern Chile (18 S–30 S): An application of error-in-variables regression to the oxygen and hydrogen stable isotope ratio of precipitation. Water 11 (4), 791.

Bozkurt, D., Rojas, M., Boisier, J.P., Valdivieso, J., 2018. Projected hydroclimate changes over Andean basins in central Chile from downscaled CMIP5 models under the low and high emission scenarios. Clim. Change 150 (3–4), 131–147. https://doi.org/10.1007/s10584-018-2246-7.

Brenning, A., Gruber, S., Hoelzle, M., 2005. Sampling and statistical analyses of BTS measurements. Permafr. Periglac. Process. 16, 383–393. https://doi.org/10.1002/ppp.541.

Carroll, R.W.H., Deems, J.S., Niswonger, R., Schumer, R., Williams, K.H., 2019. The importance of interflow to groundwater recharge in a snowmelt-dominated headwater basin. Geophys. Res. Lett. 46 (11), 5899–5908.

Cheng, G.D., Jin, H.J., 2013. Groundwater in the permafrost regions on the Qinghai-Tibet Plateau and it changes. Hydrogeol. Eng. Geol. 40 (1), 1–10.

Clark, I.D., Fritz, P., 1997. Environmental isotopes in hydrogeology. CRC Press, New York.

Cochand, M., Molson, J., Barth, J.A.C., van Geldern, R., Lemieux, J.M., Fortier, R., Therrien, R., 2020. Rapid groundwater recharge dynamics determined from hydrogeochemical and isotope data in a small permafrost watershed near Umiujaq (Nunavik, Canada). Hydrgeol. J. 28 (3), 853–868. https://doi.org/10.1007/s10040-020-02109-x.

Cooper, R., Hodgkins, R., Wadham, J., Tranter, M., 2011. The hydrology of the proglacial zone of a high-Arctic glacier (Finsterwalderbreen, Svalbard): Sub-surface water fluxes and complete water budget. J. Hydrol. 406 (1–2), 88–96.

Coplen, T.B., 1994. Reporting of stable hydrogen, carbon, and oxygen isotopic abundances (technical report). Pure Appl. Chem. 66 (2), 273–276.

Craig, H., Gordon, L.I., Horibe, Y., 1963. Isotopic exchange effects in the evaporation of water: 1. Low-temperature experimental results. J. Geophys. Res. 68 (17), 5079–5087.

Cuthbert, M.O., Gleeson, T., Moosdorf, N., Befus, K.M., Schneider, A., Hartmann, J., Lehner, B., 2019. Global patterns and dynamics of climate–groundwater interactions. Nat. Clim. Chang. 9 (2), 137–141.

Czuppon, G., Bottyán, E., Kristóf, E., Weidinger, T., Haszpra, L., Kármán, K., 2021. Stable isotope data of daily precipitation during the period of 2013–2017 from K-puszta (regional background monitoring station). Hungary. Data in Brief 36, 106962.

DGA-Arcadis, 2015. Diagnóstico de disponibilidad hídrica en cuencas Alto-Andinas de la Región de Atacama. fase 2.

Dietermann, N., Weiler, M., 2013. Spatial distribution of stable water isotopes in alpine snow cover. Hydrol. Earth Syst. Sci. 17, 2657–2668. https://doi.org/10.5194/hess-17-2657-2013.
Drusch, M., Del Bello, U., Carlier, S., Colin, O., Fernandez, V., Gascon, F., Hoersch, B., Isola, C., Laberinti, P., Martimort, P., 2012. Sentinel-2: ESA's optical high-resolution mission for GMES operational services. Remote Sens. Environ. 120, 25–36.
Enguita, P., 2016. Diagnóstico de disponibilidad hídrica en cuencas Alto-Andinas de la Región de Atacama, fase 3, AMPHOS Chile.
Eppelbaum, L., Kutasov, I., Pilchin, A., 2014. Applied Geothermics. Springer-Verlag, Berlin Heidelberg.
Evans, S.G., Ge, S., 2017. Contrasting hydrogeologic responses to warming in permafrost and seasonally frozen ground hillslopes. Geophys. Res. Lett. 44 (4), 1803–1813. https://doi.org/10.1002/2016GL072009.
Gat, J.R., 1995. Stable Isotopes of Fresh and Saline Lakes. In: Lerman, A., Imboden, D.M., Gat, J.R. (Eds.) Physics and Chemistry of Lakes. Springer, Berlin, Heidelberg. https://doi.org/10.1007/978-3-642-85132-2_5.
Gibson, J.J., Birks, S.J., Yi, Y., 2016. Higher tritium concentrations measured in permafrost thaw lakes in northern Alberta. Hydrol. Process. 30 (2), 245–249.
Giggenbach, W.F., 1992. Isotopic shifts in waters from geothermal and volcanic systems along convergent plate boundaries and their origin. Earth Planet. Sci. Lett. 113, 495–510.
Gjorup, D.F., Francelino, M.R., Michel, R.F.M., Senra, E.O., Schaefer, C.E.G.R., 2019. Pedoclimate monitoring in the periglacial high mountain soils of the Atacama Desert, northern Chile. Permafr. Periglac. Process. 30, 310–329.
Goyanes, G., Vieira, G., Caselli, A., Cardoso, M., Marmy, A., Santos, F., Bernardo, I., Hauck, C., 2014. Local influences of geothermal anomalies on permafrost distribution in an active volcanic island (Deception Island, Antarctica). Geomorphology 225, 57–68.
Grosjean, M., Geyh, M.A., Messerli, B., et al., 1995. Late-glacial and early Holocene lake sediments, ground-water formation and climate in the Atacama Altiplano 22–24°S. J Paleolimnol 14, 241–252. https://doi.org/10.1007/BF00682426.
Hammond, J.C., Harpold, A.A., Weiss, S., Kampf, S.K., 2019. Partitioning snowmelt and rainfall in the critical zone: effects of climate type and soil properties. Hydrol. Earth Syst. Sci. 23 (9), 3553–3570. https://doi.org/10.5194/hess-23-3553-2019.
Hiyama, T., Asai, K., Kolesnikov, A.B., Gagarin, L.A., Shepelev, V.V., 2013. Estimation of the residence time of permafrost groundwater in the middle of the Lena River basin, eastern Siberia. Environ. Res. Lett. 8 (3), 35040.
Houston, J., 2007. Recharge to groundwater in the Turi Basin, northern Chile: an evaluation based on tritium and chloride mass balance techniques. J. Hydrol. 334 (3–4), 534–544.
Houston, J., Hartley, A.J., 2003. The central Andean west-slope rainshadow and its potential contribution to the origin of hyper-aridity in the Atacama Desert. Int. J. Climatol. 23 (12), 1453–1464.
Ishikawa, M., 2003. Thermal regimes at the snow-ground interface and their implications for permafrost investigation. Geomorphology 52 (1–2), 105–120. https://doi.org/10.1016/S0169-555X(02)00251-9.
Jordan, T.E., Herrera, C., Godfrey, L.V., Colucci, S.J., Gamboa, C., Urrutia, J., Paul, J.F., 2019. Isotopic characteristics and paleoclimate implications of the extreme precipitation event of March 2015 in northern Chile. Andean Geol. 46 (1), 1–31.
Kaplan, G., Avdan, U., 2017. Object-based water body extraction model using Sentinel-2 satellite imagery. Eur. J. Remote Sensing 50 (1), 137–143.
Kereszturi, Á., Aszalos, J.M., Heiling, Z.s., Igneczi, Á., Kapui, Z.s., Király, C.s., Leél-Össy, S.z., Szalai, Z., Zs, N., Pál, B., Skultéti, A., Nagy, B., 2022. Wind-snow interactions at the Ojos del Salado region as a potential Mars analogue site in the Altiplano - Atacama desert region. Icarus 378, 15.
Kinnard, C., Ginot, P., Surazakov, A., MacDonell, S., Nicholson, L., Patris, N., Squeo, F.A., 2020. Mass balance and climate history of a high-altitude glacier, Desert Andes of Chile. Front. Earth Sci. 8, 40.
Kull, C., Grosjean, M., Veit, H., 2002. Modelling modern and Late Pleistocene glacio-climatological conditions in the North Chilean Andes (29-30°S). Clim. Change 52 (2), 359–381.
LeCun, Y., Bengio, Y., Hinton, G., 2015. Deep Learning. Nature 521 (7553), 436–444.
Lobos-Roco, F., Hartogensis, O., Vilà-Guerau de Arellano, J., de la Fuente, A., Muñoz, R., Rutllant, J., Suárez, F., 2021. Local evaporation controlled by regional atmospheric circulation in the Altiplano of the Atacama Desert. Atmos. Chem. Phys. 21 (11). https://doi.org/10.5194/acp-21-9125-2021.
Lucas, L., Unterweger, M., 2000. Comprehensive Review and Critical Evaluation of the Half-Life of Tritium. J. Res. Natl. Inst. Stand. Technol. 105 (4), 541–549. https://doi.org/10.6028/jres.105.043.
Markovich, K.H., Manning, A.H., Condon, L.E., McIntosh, J.C., 2019. Mountain-block recharge: a review of current understanding. Water Resour. Res. 55 (11), 8278–8304.
Masiokas, M.H., Rabatel, A., Rivera, A., Ruiz, L., Pitte, P., Ceballos, J.L., Barcaza, G., Soruco, A., Bown, F., Berthier, E., Dussaillant, I., MacDonell, S., 2020. A Review of the Current State and Recent Changes of the Andean Cryosphere. Front. Earth Sci. 8, 99. https://doi.org/10.3389/feart.2020.00099.
Masson-Delmotte, V., Zhai, P., Pirani, A., Connors, S.L., Péan, C., Berger, S., Caud, N., Chen, Y., Goldfarb, L., Gomis, M. I., Huang, M., Leitzell, K., Lonnoy, E., Matthews, J. B.R., Maycock, T.K., Waterfield, T., Yelekçi, O., R. Y., B. Z., 2021. Summary for Policymakers. in: Climate Change 2021: The Physical Science Basis. Contribution of Working Group I to the Sixth Assessment Report.
McFeeters, S.K., 1996. The use of the Normalized Difference Water Index (NDWI) in the delineation of open water features. Int. J. Remote Sens. 17 (7), 1425–1432.
Mena, G., Yoshikawa, K., Schorghofer, N., Pastén, C., Ochoa, F.A., Yoshii, Y., Doi, M., Miyata, T., Takahashi, H., Casassa, G., Sone, T., 2021. Freeze–thaw cycles and snow impact at arid permafrost region in Chajnantor Volcano, Atacama, northern Chile. Arct. Antarct. Alp. Res. 53 (1), 60–66. https://doi.org/10.1080/15230430.2021.1878739.
Nagy, B., Ignéczi, Á., Kovács, J., Szalai, Z., Mari, L., 2019. Shallow ground temperature measurements on the highest volcano on Earth, Mt. Ojos del Salado, Arid Andes, Chile. Permafrost and Periglacial Processes 30, 3–18.
Nagy, B., Kovács, J., Ignéczi, Á., Beleznai, S., Mari, L., Kereszturi, Á., Szalai, Z., 2020. The thermal behavior of ice-bearing ground: the highest cold, dry desert on Earth as an analog for conditions on Mars, at Ojos del Salado. Puna De Atacama-Altiplano Region. Astrobiology 20 (6), 701–722.
Nicholson, S., 1998. Desert hydrology. In: Encyclopedia of Hydrology and Water Resources. Springer, pp. 176–183.
Obu, J., Westermann, S., Kaab, A., Bartsch, A., 2019. Ground Temperature Map, 2000-2016, Andes, New Zealand and East African Plateau Permafrost. In University of Oslo. PANGAEA. https://doi.org/10.1594/PANGAEA.905512.
Oliva, M., Fritz, M., 2018. Permafrost degradation on a warmer Earth: challenges and perspectives. Curr. Opin. Environ. Sci. Health 5, 14–18.
Outcalt, S.I., Nelson, F.E., Hinkel, K.M., 1990. The zero-curtain effect: heat and mass transfer across an isothermal region in freezing soil. Water Resour. Res. 26 (7), 1509–1516. https://doi.org/10.1029/WR026i007p01509.
Palcsu, L., Major, Z., Köllő, Z., Papp, L., 2010. Using an ultrapure 4He spike in tritium measurements of environmental water samples by the 3He-ingrowth method. Rapid Commun. Mass Spectrom. 24, 698–704. https://doi.org/10.1002/rcm.4431.
Pena-Regueiro, J., Sebastia-Frasquet, M.-T., Estornell, J., Aguilar-Maldonado, J.A., 2020. Sentinel-2 application to the surface characterization of small water bodies in wetlands. Water 12 (5), 1487.
Ruder, S., 2016. An overview of gradient descent optimization algorithms. arXiv, 2016; arXiv:1609.04747.
Ruiz Pereira, S., Marquardt, C., Beriain, E., Lambert, F., 2021. Permafrost evolution in a mountain catchment near Santiago de Chile. J. S. Am. Earth Sci. 109, 103293.
Saavedra, F.A., Kampf, S.K., Fassnacht, S.R., Sibold, J.S., 2018. Changes in Andes snow cover from MODIS data, 2000–2016. Cryosphere 12 (3), 1027–1046.
Sjöberg, Y., Jan, A., Painter, S.L., Coon, E.T., Carey, M.P., O'Donnell, J.A., Koch, J.C., 2021. Permafrost promotes shallow groundwater flow and warmer headwater streams. Water Resour. Res. 57 (2), e2020WR027463.
Somers, L.D., McKenzie, J.M., 2020. A review of groundwater in high mountain environments. Wiley Interdiscip. Rev. Water 7 (6), e1475.
Tassi, F., Aguilera, F., Darrah, T., Vaselli, O., Capaccioni, B., Poreda, R.J., Huertas, A.D., 2010. Fluid geochemistry of hydrothermal systems in the Arica-Parinacota, Tarapacá and Antofagasta regions (northern Chile). *J. Volcanol. Geoth. Res.* 192 (1–2), 1–15.
Tazioli, A., Fronzi, D., Mammoliti, E., 2022. Tritium as a tracer of leachate contamination in groundwater: a brief review of tritium anomalies method. *Hydrology* 9 (5), 75. https://doi.org/10.3390/hydrology9050075.
van Everdingen, R., 2005. Multi-language glossary of permafrost and related ground-ice terms. International Permafrost Association.
Vargas Paysen, J., 2013. Diagnóstico de disponibilidad hídrica en cuencas Alto-Andinas de la Región de Atacama. Estudios Dirección General de Aguas, Chile.
Viviroli, D., Weingartner, R., 2008. "Water towers"—A global view of the hydrological importance of mountains. In Mountains: Sources of water, sources of knowledge. Springer, pp. 15–20.
Wan, C., Gibson, J.J., Shen, S., Yi, Y., Yi, P., Yu, Z., 2019. Using stable isotopes paired with tritium analysis to assess thermokarst lake water balances in the Source Area of the Yellow River, northeastern Qinghai-Tibet Plateau, China. Sci. Total Environ. 689, 1276–1292.
Wang, G., Hu, H., Li, T., 2009. The influence of freeze–thaw cycles of active soil layer on surface runoff in a permafrost watershed. J. Hydrol. 375 (3–4), 438–449.
Woodside, W., Messmer, J.H., 1961. Thermal conductivity of porous media. J. Appl. Phys. 32, 1688. https://doi.org/10.1063/1.1728419.
Wu, W.-Y., Lo, M.-H., Wada, Y., Famiglietti, J.S., Reager, J.T., Yeh, P.-J.-F., Ducharne, A., Yang, Z.-L., 2020. Divergent effects of climate change on future groundwater availability in key mid-latitude aquifers. Nat. Commun. 11 (1), 1–9.
Yang, X., Zhao, S., Qin, X., Zhao, N., Liang, L., 2017. Mapping of urban surface water bodies from Sentinel-2 MSI imagery at 10 m resolution via NDWI-based image sharpening. Remote Sens. (Basel) 9 (6), 596.